CHAPTER 13

# RF Test Methods

This chapter will describe the principles of RF testing of electronic circuits using commercial automated test equipment (ATE). These principles are largely based on the physical concepts related to wave propagation outlined in Chapter 12. However, these techniques also make use of the sampling principles related to DSP-based testing developed in the earlier part of this textbook. In this chapter we shall focus on the most common types of RF tests for standard devices, like mixers, VCOs, and power amplifiers, to name just a few. For devices not covered in this work, the test principles provided should be easily extendable with only minor modifications to the device or test setup. Of course, the better one understands the fundamentals of RF test, the easier it will be to adjust a given test technique to a specific problem at hand.

In an RF test, many different test types are used to decide if a device is within specification and whether it should be shipped to the customer. Below is a list of some of these methods that are being considered for a production-oriented RF test by the research community:

- Structural test
- Functional test
- Observer (model)-based test, which includes testing against a regression
- Specification-based test
- Correlation-based test (alternate test)
- Defect-oriented test
- Build-in test (BIT) and Build-in self-test (BIST)
- Statistical-based test (e.g., BER, EVM)

While the research community continues to search for the most effective approach, this chapter is limited to a discussion related to functional or specification-based testing with some discussion about observer-based and statistical-based testing. In a later chapter, we will provide some discussion about BIST and BIT for RF devices, as well as correlation-based test. However, for the most part, these techniques are still early ideas and further work is required before they are declared ready for production test. Nonetheless, the test engineer needs to be exposed to early ideas in order to be better understand present-day test problems and possible directions from which solutions will appear.

One operation that is common to all product-oriented RF tests is the measurement of power and phase related to single or multiple sinusoidal waves. Generally, such measurements are made through the capture of the time-domain information using a digitizing operation, followed by an FFT to determine the frequency domain description of the signal. Our readers at this stage of the textbook should be able to fully understand this approach and the advantages it offers the test engineer. For those readers who skipped ahead to this chapter, they should consider reviewing Chapters 8–11 before reading this chapter.

This chapter will begin with a description of the general architecture of the RF section of the ATE. This will help provide a better understanding of how power measurements are made, as well as their limitations. Subsequently, we will describe various RF test metrics like power gain, intermodulation distortion, harmonics, noise figure, and phase noise. In this chapter we will also learn about some statistical test metrics that apply at the system level, like bit error rate (BER) and error vector magnitude (EVM) test measures.

When developing an understanding of RF test techniques, it is important to think of the RF portion of the ATE as an RF system unto itself. In this way, it is easier to encapsulate an understanding of the system operation based on maximum power limitations, linear power range, noise floor, dynamic range, gain, bandwidth and phase noise. These limitations are common to all RF systems and will continue to play a role in the RF test technique of subsequent chapters.

## 13.1 SCALAR MEASUREMENT METHODS

The scalar power measurement is the basis for a large number of RF test techniques used in production. In this section, we will discuss the principles and the limitations of a scalar power measurement made with an ATE, and we will compare them to the methods used in focus bench equipment found in characterization laboratories.

### 13.1.1 Principles of a Scalar Power Measurement

Let us look at the three common methods used to extract a power signal and, correspondingly, extract a power metric. This will include a discussion of the principles and limitations of a (a) calorimetric power sensor, (b) superheterodyne power sensor, and (c) zero-IF (intermediate frequency) with sampling power sensor.

#### *Calorimetric Power Sensor*

A power meter constructed with calorimetric and bolometric power sensors, also referred to as thermocouples, measure the true heating power of an RF signal. As shown in Figure 13.1, the RF power is transformed into an equivalent thermal power and detected with a temperature

**Figure 13.1.** Simple calorimetric set-up for accurate RF power measurement.

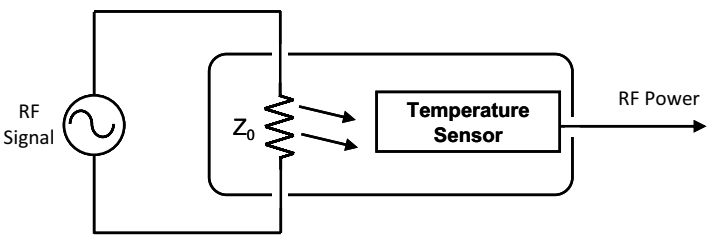

sensor by terminating the power source, here depicted as RF source, with a resistor with the real impedance $Z_0$. The signal from the temperature sensor is processed and displayed. These calorimetric sensors are very accurate and measure the RF power, including the noise floor, harmonics, spurious, and the signal itself in the measurement bandwidth of the power sensor. This technique is used in most RF power meters. These methods are very accurate with respect to the true RMS power of a signal, even for complex signal types. However, they have some serious limitations at low power levels as both the signal and the noise are combined into one power number. A related approach is based on computing the RMS value of a power signal electrically through an integration operation. Such instruments are limited in accuracy when measuring complex signals with a high crest factor or a complex duty cycle in contrast to calorimetric sensors.

### *Superheterodyne Power Sensor*

Superheterodyne instruments measure power with a power sensor comparable to a spectrum analyzer. The principal architecture of these spectrum analyzers are based on the input stage of a traditional FM radio, which includes a mixer, an IFamplifier with an IFtracking filter, and a power detector as shown in Figure 13.2. While sweeping the center frequency of the IF-tracking filter with a sweeping generator over a predetermined range of frequencies, a spectrum analyzer is capable of measuring signal power as a function of the frequency (as opposed to power as a function of time). With the pre-selector filter together with the tracking filter, a spectrum analyzer is capable of limiting the bandwidth of the measured signal, which increases the measurement dynamic range significantly compared to a power meter. With this architecture, input bandwidths as high as 30 GHz can be measured, because only a small frequency range is measured at any one time. This has the added benefit that background noise levels appearing at the input will not compress or saturate the IF log amplifier and detector stages of the analyzer. The use of a logarithmic amplifier provides the instrument with the capability to separate signals that differ in signal strength by over 90 dB. On account of its versatility, the spectrum analyzer is standard equipment for bench characterization of various parameters requiring power measurements in the frequency domain.

**Figure 13.2.** Block diagram of a typical superheterodyne spectrum analyzer.

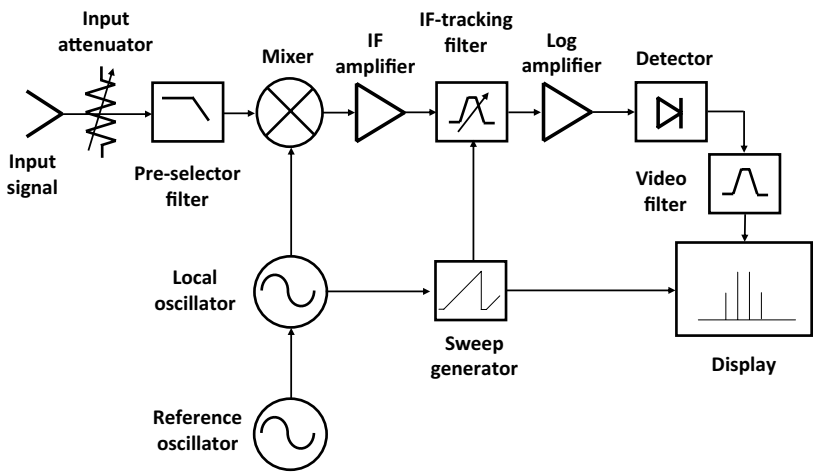

### *Zero-IF with Sampling Power Sensor*

The architecture of a typical ATE power meter is much simpler than that seen for the superheterodyne spectrum analyzer. Most testers are built with what is referred to as a zero-IF (ZIF) architecture followed by an ADC to convert the IF signal into a digital signal as a function of time for further digital signal processing. A block diagram of the ZIF architecture can be seen in Figure 13.3. Some systems have a second IF stage to suppress spurious responses and allow for additional filtering. The mixer is a non-image reject mixer, one that generates both the in-band signal and its image. The overall bandwidth of the instrument is limited by the bandwidth of the front-end low-noise amplifier (LNA), as well by as the bandwidth of the IF stage and, possibly, the ADC. Typical input bandwidths found on commercial ATEs are about 6 GHz. It is important to note that the instrument described here based on the ZIF architecture performs measurements in the time domain on voltage samples presented to the ADC and converts this information into a power signal as a function of frequency using a FFT. This operation is clearly quite different from that which is performed by a spectrum analyzer.

Let us assume that an $N$-point data sequence $x[n]$ corresponds to the voltage signal appearing at the input to the ADC. Subsequently, an $N$-point FFT analysis is performed on this data set. As we learned in Chapter 10, the RMS value of the spectral coefficients $c_k$ corresponding to this data set can be written in the usual way as

$$c_{k,RMS} = \begin{cases} \left|Y\left[k\right]\right|, & k = 0 \\ \sqrt{2}\left|Y\left[k\right]\right|, & k = 0,\ldots,N/2-1 \\ \dfrac{\left|Y\left[k\right]\right|}{\sqrt{2}}, & k = N/2 \end{cases} \tag{13.1}$$

where

$$Y = \frac{FFT\left\{x\left[n\right]\right\}}{N}$$

The power in each bin can then be found by simply squaring each $c_{k,RMS}$ term above and normalized by the appropriate real-valued input impedance level $Z_0$ associated with the ADC. Generally, $Z_0$ is

**Figure 13.3.** Block diagram of a typical ZIF ATE measurement path architecture.

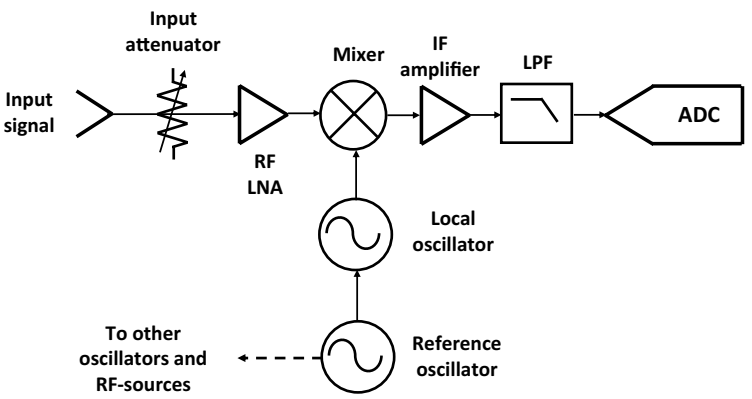

a standardized value of 50 Ω. For example, if the signal A is located in bin $M_A$ and another signal B is located in bin $M_B$, then the power in dBm associated with each term is computed according to

$$P_{S_A}\Big|_{\text{dBm}} = 10\log_{10}\left[\frac{C_{M_A,\,RMS}^2 / Z_0}{1\,\text{mW}}\right] \tag{13.2}$$

and

$$P_{S_B}\Big|_{\text{dBm}} = 10\log_{10}\left[\frac{C_{M_B,\,RMS}^2 / Z_0}{1\,\text{mW}}\right] \tag{13.3}$$

An important limitation of the ZIF architecture is the requirement for a front-end LNA with large input signal bandwidth, a low-noise figure, a high compression point, and a low intermodulation distortion level (more on these two in moment). On account of the design difficulties of achieving all these specifications simultaneously, the LNA becomes the critical component of this instrument and often limits the smallest power level that can be measured. Another limitation of the ZIF architecture is the conversion range associated with the ADC. For small signals in the presence of a carrier, or some other large signal, the ADC must be capable of digitizing both the large and the small signals simultaneously. A similar argument can be made for measuring the phase noise associated with a signal; a large signal component carries a small signal in the form of a phase modulation. Of course, the ADC has a limited resolution, which ultimately limits the dynamic range of signals that it can convert. Another issue is, of course, the need for coherency between the measured IF signal and the sampling clock of the ADC. Generally, this is handled by setting the frequency of the local oscillator (LO) such that the measured signal frequency falls directly into a bin of the FFT. Since there is no settling time associated with the sampling process (as long as the signal is within the ADC bandwidth), the ZIF architecture leads to quicker test time than the spectrum analyzer architecture.

An important aspect of any power measurement regardless of the instrument's internal architecture is to establish the correct signal level at its input so that the system produces an output signal that is of the highest quality representation possible, i.e., one with highest accuracy. On the one hand, a large signal will maintain a large signal-to-noise ratio but will, simultaneously, result in a low signal-to-distortion ratio. The net result is poor measurement accuracy. On the other hand, a small signal will result in a low signal-to-noise ratio but a large signal-to-distortion ratio. Again, the net result is poor measurement accuracy. Somewhere in between a large signal input and a small signal input will result in the optimum input situation. It is the goal of the test engineer to establish these optimum signal conditions so each and every measurement is made with the right amount of accuracy. This is achieved with an attenuator at the front end of the instrument (see, for instance, Figure 13.3) whose gain is set by the test engineer according to the maximum expected level of power involved in the measurement.

In the context of an RF power measurement, we can see that these effects trade off in terms of the signal spectrum appearing at the output of the instrument. Let us assume that the input power signal consists of two independent tones. If the input peak power level is set too low through a large amount of attenuation, then the output of the instrument will consist of two very small-sized tones, positioned very close to the instrument noise floor, as illustrated in Figure 13.4a. If the attenuation is reduced, then higher level tones would be present at the instrument output, as seen in the spectrum of Figure 13.4b. At the optimum attenuation setting, some distortion caused by the instrument will just start to appear along side the two input tones produced by the DUT. If the attenuation is further reduced, then the two input tones will cause the instrument to compress, whereby the signal level of the two tones will decrease, the noise floor level will decrease and, in addition, higher distortion products will appear at the instrument output. This situation is depicted

**Figure 13.4.** Impact of expected power level setting on the signal, distortion and noise level: (a) expected power level set too high, (b) expected power level set correct, (c) expected power level set too low.

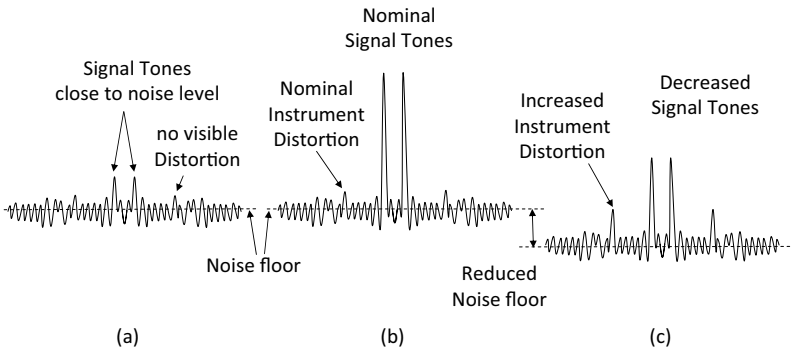


in Figure 13.4c. This problem is further complicated by the calibration procedure that follows the measurement. Since calibration factors are generated in terms of the attenuation level selected, if additional attenuation occurs through the instrument on account of compression, the calibration process will be in error, greatly reducing the accuracy of the measurement.

When testing the power of a known signal, it is important to know the full spectrum, as well as any time dependency, since out-of-band and unwanted signals can compress the measurement path in the same manner as the measurement signal. In the case of small signals, one can find that the wideband noise associated with the signal can cause the instrument to compress if the attenuator is not set properly. For large power signals, the crest factor of the signal, which includes multiple tones as well, must be taken into account. For example, in Section 13.2.4 we learned that the average or burst power in a given frame for a WLAN OFDM signal is 11 dB lower than its peak power. In this case, it is necessary to set the maximum expected power 11 dB higher than the burst power.

Commercial ATE RF power instruments are typically built according to the ZIF architecture shown in Figure 13.3. Like most ATE instruments, they are based on sampling and require coherent operation for best operation. In general, this might require synchronizing the DUT timing to the timing base of the ATE. Moreover, coherency requires that the incoming signal frequency to the ADC, denoted by $f_{IF}$, be related to the ADC sampling rate $F_S$ according to

$$f_{IF} = \frac{M}{N} F_S \tag{13.4}$$

where $N$ is the number of samples collected by the sampling process and $M$ corresponds to the FFT bin in which the incoming signal will fall. Here we denote the ADC input frequency as that corresponding to the intermediate frequency associated with the mixer output, that is, $f_{IF}$. To have all signal power within one FFT bin, $M$ must be an integer. When $M$ is not an integer, some of the signal power will be distributed over multiple bins, causing frequency leakage and possible measurement error. This becomes even more problematic when testing for the phase noise of a signal, since the contribution of the phase noise of the signal and the power leakage cannot be separated. These two test situations are illustrated in the FFT plots shown in Figure 13.5. The top plot illustrates the noncoherent sampling situation and the bottom plot illustrates the desired coherent sampling situation.

**Figure 13.5.** A comparison of a non-coherent test situation (a) with a test condition that is coherent (b).

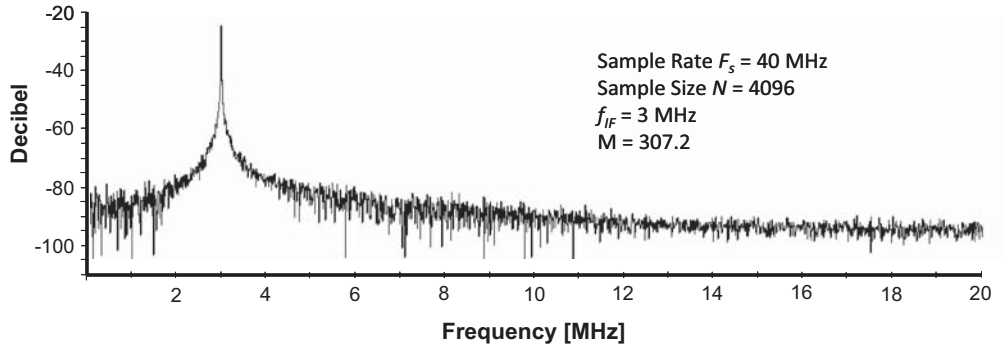


(a)

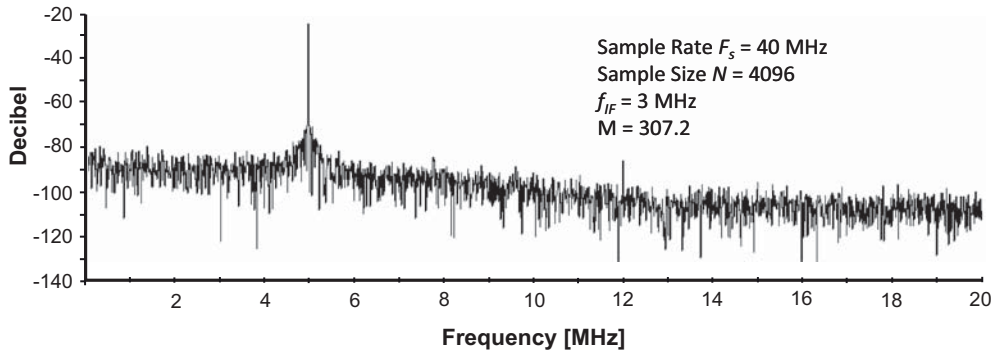


(b)

As the ADC input is derived from the output of the mixer, it is, in turn, related to the local oscillator frequency $f_{LO}$. The input frequencies to the mixer $f_{RF}$ and $f_{LO}$ are related to its output intermediate frequency $f_{IF}$ according to

$$f_{IF} = f_{LO} - f_{RF} \tag{13.5}$$

or

$$f_{IF} = f_{RF} - f_{LO} \tag{13.6}$$

The case of Eq. (13.5) is low-side injection (the frequency of the RF signal is lower than the LO frequency), and for Eq. (13.6), it is high-side injection. Substituting Eq. (13.4) into Eq. (13.5) the LO frequency is

$$f_{LO} = \frac{M}{N} F_S + f_{RF} \tag{13.7}$$

or substituting Eq. (13.4) into Eq. (13.6), the LO frequency is

$$f_{LO} = \frac{M}{N} F_S - f_{RF} \tag{13.8}$$

Because the RF test signal frequency is, in general, arbitrary in value, we find from the above expression that the LO frequency will also have to be an arbitrary in value, even though the ADC input is constrained to a finite set of discrete frequencies. Fortunately, on ATEs, the LO is a continuous wave oscillator and is therefore not constrained to any finite set of frequencies. This, in turn, makes it a straightforward exercise to develop a frequency plan to have all single-frequency RF signals sampled coherently.

## EXAMPLE 13.1

What IF frequency should be selected for a ZIF ATE architecture to be coherent with an ADC having a sampling rate of 20 MHz and 1024 samples are required for FFT processing.

**Solution:**
With $N = 1024$, the Fourier frequency will be given by

$$F_f = \frac{F_S}{N} = \frac{20\,\text{MHz}}{1024} = 19{,}531.250\,\text{Hz}$$

As the IF frequency must be a multiple of $F_f$, we select a value for $M$ such that it shares no common factors with $N$; that is, let $M = 511$, then

$$f_{IF} = M \cdot \frac{F_S}{N} = 511 \cdot \frac{20\,\text{MHz}}{1024} = 9.9805\,\text{MHz}$$

Therefore an IF frequency of 9.9805 MHz is required for coherent sampling.

### 13.1.2 Gain Measurement

Device gain is one of the standard tests for RF devices. Figure 13.6 illustrates a typical ATE arrangement. Here, we assume that the more general term "gain" is used as a synonym for the available gain of the DUT, defined as follows:

$$G_A = \frac{\text{power available from output line, } P_{OUT}}{\text{power available from source, } P_A} \tag{13.9}$$

where we replaced the word network by output line to be specific to the problem at hand. Here available power simply refers to the network situation where the power transfer is maximized, that is, source and load are conjugate matched. We learned in Section 12.4.2 that not all the power available from the source will make its way to the input of the DUT, because some of this power will be reflected and dissipated by the DUT interface board and the DUT itself. Also, the power leaving the DUT will experience similar losses as it makes it way to the power meter or load. It will be required to de-embed the DUT performance from the measured performance. Therefore, we modify the definition of available gain to account for this loss and write the desired device gain $G_A'$ as

$$G_A' = \frac{\text{power available from DUT, } P_{OUT,DUT}}{\text{power available from input line, } P_{IN,DUT}} \tag{13.10}$$

**Exercises**

**13.1.** What IF frequency should be selected for a ZIF ATE architecture to be coherent with an ADC having a sampling rate of 100 MHz, if 20ww48 samples are required for FFT processing and the output of the mixer ranges between 25 and 50 MHz?

ANS. For $M = 615$, $f_{IF} = 30.029$ MHz

**13.2.** A 1-GHz RF signal is to be down converted by a mixer and directed to a digitizer for digital conversion. If the digitizer is sampled at a clock rate of 100 MHz and 4096 samples are collected for digital signal processing using an FFT, what should be the local oscillator frequencyif the mixer has an output IF frequency range between 40 and 60 MHz?

ANS. $f_{LO} = 987.52$ MHz for $M = 511$.

By introducing the power gain of the interface board or, for that matter, any lossy RF line, we can define the ***input operating gain***, $G_{o,IN}$, of the source-DUT interconnect as the ratio of the power made available to the input of the DUT to the power available from the source, that is,

$$G_{o,IN} = \frac{\text{power available from input line, } P_{IN,DUT}}{\text{power available from source, } P_A} \tag{13.11}$$

In a similar manner, we can define the ***output operating gain***, $G_{o,IN}$, of the DUT-load interconnect as the ratio of the power made available at the load to the power made available by the DUT, that is,

$$G_{o,OUT} = \frac{\text{power available from output line, } P_{OUT}}{\text{power available from DUT, } P_{OUT,DUT}} \tag{13.12}$$

Collectively, these three power gains are combined according to

$$G_A = G_{o,IN} \cdot G'_A \cdot G_{o,OUT} \tag{13.13}$$

Expressing this relationship in terms of decibels, we write

$$G_A\big|_{\text{dB}} = G_{o,IN}\big|_{\text{dB}} + G'_A\big|_{\text{dB}} + G_{o,OUT}\big|_{\text{dB}} \tag{13.14}$$

Finally, our end goal is to determine $G'_A$; rearranging Eq. (13.14), we write

$$G_A\big|_{\text{dB}} = G_{o,IN}\big|_{\text{dB}} + G'_A\big|_{\text{dB}} + G_{o,OUT}\big|_{\text{dB}} \tag{13.15}$$

Because $G'_A$ and $G_{o,OUT}$ are always less than one for passive lines, it is customary to speak in terms of a loss, so the two rightmost terms, including its sign, is encapsulated into a new term called the ***operating loss***, *OL*, expressed in decibels, as

$$G'_A\big|_{\text{dB}} = G_A\big|_{\text{dB}} + \text{OL}\big|_{\text{dB}} \tag{13.16}$$

**Figure 13.6.** ATE gain test setup with interface board.

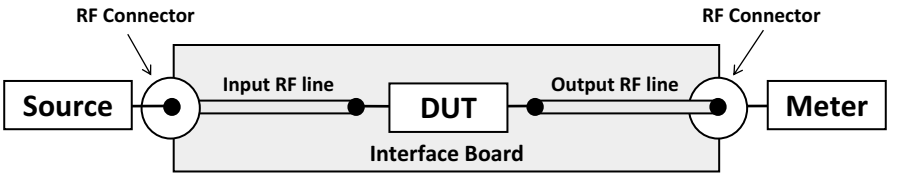


where

$$\mathrm{OL}\big|_{\mathrm{dB}} = -10\cdot\log_{10}\left(G_{o,IN}\right) - 10\cdot\log_{10}\left(G_{o,OUT}\right) \tag{13.17}$$

We can therefore conclude that to acquire the gain of a device with an ATE accurately, one must first account for the operating loss of the device interface board and any reflective effects associated with the DUT or meter.

One approach that is commonly used to estimate the operating losses is from the mismatch losses associated with the DUT. Using a calibrated network analyzer the input and output return loss of the DUT, together with the DIB, source, and meter, can be determined from which the mismatch loss associated with the input source-DUT signal path, denoted by $\mathrm{ML}_{S-DUT}$, can be computed (see, for example, Eq. (12.117) in Chapter 12). Likewise, the mismatch loss associated with the DUT-meter signal path, denoted by $\mathrm{ML}_{DUT-M}$, can be computed. The mismatch loss of the DUT, together with the any dissipative or other losses associated with the cables and traces on the input and output side of the DUT, denoted by $\mathrm{ML}_{LINE-IN}$ and $\mathrm{ML}_{LINE-OUT}$, respectively, can be approximately combined in a linear manner to provide an estimate of the operating losses of the test setup. Recalling that each mismatch loss is expressed in terms of a bound, we must write the operating loss in the following manner:

$$\begin{aligned}&\min\left\{\mathrm{ML}_{S-DUT}\big|_{\mathrm{dB}}\right\}+\min\left\{\mathrm{ML}_{LINE-IN}\big|_{\mathrm{dB}}\right\}+\\&\min\left\{\mathrm{ML}_{LINE-OUT}\big|_{\mathrm{dB}}\right\}+\min\left\{\mathrm{ML}_{DUT-M}\big|_{\mathrm{dB}}\right\}\end{aligned} \le \mathrm{OL}_{\mathrm{dB}} \le \begin{aligned}&\max\left\{\mathrm{ML}_{S-DUT}\big|_{\mathrm{dB}}\right\}+\max\left\{\mathrm{ML}_{LINE-IN}\big|_{\mathrm{dB}}\right\}+\\&\max\left\{\mathrm{ML}_{LINE-OUT}\big|_{\mathrm{dB}}\right\}+\max\left\{\mathrm{ML}_{DUT-M}\big|_{\mathrm{dB}}\right\}\end{aligned} \tag{13.18}$$

Any uncertainty associated with the mismatch loss parameter would translate to uncertainty in the operating loss parameters, which, in turn, leads to uncertainty in the gain term given by

$$\Delta G'_A\big|_{\mathrm{dB}} = \mathrm{MU}_{S-DUT}\big|_{\mathrm{dB}} + \mathrm{MU}_{DUT-M}\big|_{\mathrm{dB}} + \mathrm{MU}_{LINE-IN}\big|_{\mathrm{dB}} + \mathrm{MU}_{LINE-OUT}\big|_{\mathrm{dB}} \tag{13.19}$$

where each uncertainty term is given by

$$\begin{aligned}\mathrm{MU}_{S-DUT}\big|_{\mathrm{dB}} &= \max\left\{\mathrm{ML}_{S-DUT}\big|_{\mathrm{dB}}\right\} - \min\left\{\mathrm{ML}_{S-DUT}\big|_{\mathrm{dB}}\right\}\\ \mathrm{MU}_{DUT-M}\big|_{\mathrm{dB}} &= \max\left\{\mathrm{ML}_{DUT-M}\big|_{\mathrm{dB}}\right\} - \min\left\{\mathrm{ML}_{DUT-M}\big|_{\mathrm{dB}}\right\}\\ \mathrm{MU}_{LINE-IN}\big|_{\mathrm{dB}} &= \max\left\{\mathrm{ML}_{LINE-IN}\big|_{\mathrm{dB}}\right\} - \min\left\{\mathrm{ML}_{LINE-IN}\big|_{\mathrm{dB}}\right\}\\ \mathrm{MU}_{LINE-OUT}\big|_{\mathrm{dB}} &= \max\left\{\mathrm{ML}_{LINE-OUT}\big|_{\mathrm{dB}}\right\} - \min\left\{\mathrm{ML}_{LINE-OUT}\big|_{\mathrm{dB}}\right\}\end{aligned} \tag{13.20}$$

## EXAMPLE 13.2

A gain test was performed on a DUT using an ATE with an interface board as shown in Figure 13.6. The source and power meter is located in the ATE. The return loss of the source and meter are known to be 15 and 21 dB, respectively. A network analyzer was used to measure the return loss of the input and output port of the DUT to be 10 and 12 dB, respectively. The PCB designer found through simulation that the traces and connectors introduce losses of about 0.5 dB equally on both sides of the DUT. If the ratio of the output available power to input available power was found to be 12.4 dB, what is the device gain when the board and reflective losses are taken into account?

**Solution:**
The reflection coefficient of the source, power meter, and DUT is found according to

$$\rho_S = 10^{-RL[\text{dB}]/20} = 10^{-15/20} = 0.1778$$
$$\rho_M = 10^{-RL[\text{dB}]/20} = 10^{-21/20} = 0.0892$$
$$\rho_{IN} = 10^{-RL[\text{dB}]/20} = 10^{-10/20} = 0.3162$$
$$\rho_{OUT} = 10^{-RL[\text{dB}]/20} = 10^{-12/20} = 0.2512$$

The expected level of mismatch loss on the DUT input side of the interconnect can be bounded using the theory of Chapter 12, Section 12.4.2, repeated here for convenience as

$$\frac{\left(1-\rho_S\cdot\rho_{IN}\right)^2}{\left(1-\rho_S^2\right)\cdot\left(1-\rho_{IN}^2\right)} \le \text{ML}_{S-DUT} \le \frac{\left(1+\rho_S\cdot\rho_{IN}\right)^2}{\left(1-\rho_S^2\right)\cdot\left(1-\rho_{IN}^2\right)}$$

Substituting the appropriate values, we find

$$0.0944\ \text{dB} \le \text{ML}_{S-DUT}\big|_{\text{dB}} \le 1.072\ \text{dB}$$

Repeating for the interconnect on the output side of the DUT, we obtain

$$\frac{\left(1-\rho_{OUT}\cdot\rho_M\right)^2}{\left(1-\rho_{OUT}^2\right)\cdot\left(1-\rho_M^2\right)} \le \text{ML}_{DUT-M} \le \frac{\left(1+\rho_{OUT}\cdot\rho_M\right)^2}{\left(1-\rho_{OUT}^2\right)\cdot\left(1-\rho_M^2\right)}$$

or

$$0.121\ \text{dB} \le \text{ML}_{DUT-M}\big|_{\text{dB}} \le 0.510\ \text{dB}$$

Subsequently, we compute the operating loss using Eq. (13.18) with the appropriate values substituted according to

$$0.0944\ \text{dB} + 0.5\ \text{dB} + 0.5\ \text{dB} + 0.121\ \text{dB} \le \text{OL}\big|_{\text{dB}} \le 1.072\ \text{dB} + 0.5\ \text{dB} + 0.5\ \text{dB} + 0.510\ \text{dB}$$

which reduces to

$$1.215\ \text{dB} \le \text{OL}\big|_{\text{dB}} \le 2.582\ \text{dB}$$

Finally, using Eq. (13.16), we can estimate the actual DUT gain to be

$$12.4\ \text{dB} + 1.215\ \text{dB} \le G'_A\big|_{\text{dB}} \le 12.4\ \text{dB} + 2.582\ \text{dB}$$

which further reduces to

$$13.61\ \text{dB} \le G'_A\big|_{\text{dB}} \le 14.98\ \text{dB}$$

The available gain of the device is therefore bounded between 13.61 dB and 14.98 dB when the interface board and DUT reflection losses are account for.

An alternative approach is to characterize the lossy line with a set of *S*-parameters, in much the same way that any two-port network would be characterized. Consider that a source is connected to a load through a lossy RF line. In addition, we shall assume that the lossy line is physically separated from the source and the load by two other unspecified transmission lines as shown in Figure 13.7a. We can then model this situation with the electrical wave network shown in Figure 13.7b. Here the lossy RF line is modeled with a set of *S*-parameters, denoted by $\{S_{11}, S_{12}, S_{21}, S_{22}\}$ and a set of reflection coefficients $\{\Gamma_S, \Gamma_{IN}, \Gamma_{OUT}, \Gamma_L\}$ established at the plane of discontinuities at the input and output ports of the lossy RF line, as indicated in Figure 13.7b. The specifics of the two other transmission lines are not important, because their effects are fully accounted for by the source and load reflection coefficients.

In order to measure the waves at both the input and output port of the lossy RF line, connectors must be inserted into the signal path at each end in order for the network analyzer to gain access to these waves. However, in many test situations this may not be possible or even desirable. Instead, a method that makes measurements at one end of the lossy line where a connector is generally available is preferred. This method makes use of several carefully calibrated standard loads that are inserted into a socket at the load end of the line hence giving rise to the name ***in-socket calibration method***. These standards include a short circuit, open circuit and a 50 Ω load. Since passive networks are generally reciprocal—that is, operate exactly the same way if the source and load is interchanged—the forward and reverse transmission coefficients of the *S*-parameter description are equal, that is, $S_{12} = S_{21}$. This implies that the lossy RF line model consists of only three unknown parameters. Through the application of three separate measurements (involving

**Figure 13.7.** (a) Illustrating the physical separation between a source, lossy RF line and a load. (b) A two-port equivalent representation of the lossy RF line with corresponding reflection coefficients shown.

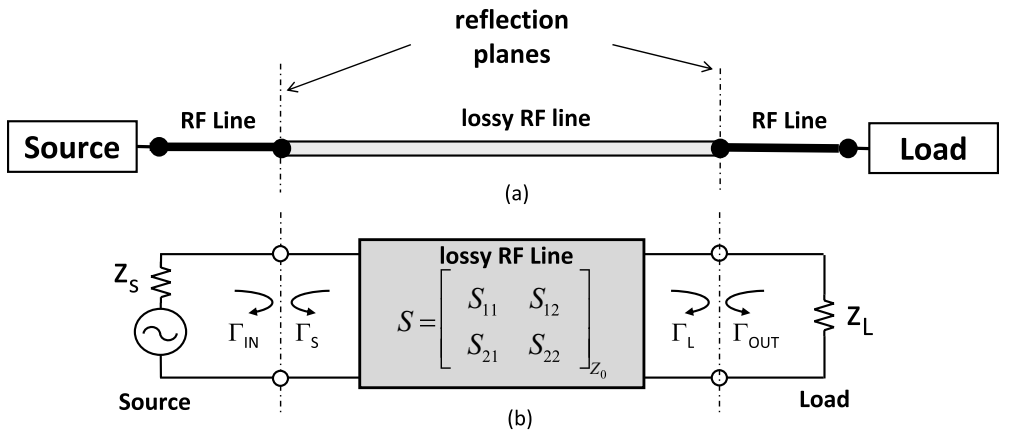

**Figure 13.8.** Making measurements at input port of lossy RF line using the in-socket calibration method: (a) The three terminating conditions for establishing the Sparameters of the lossy RF line. (b) Load with $Z_{DUT}$.

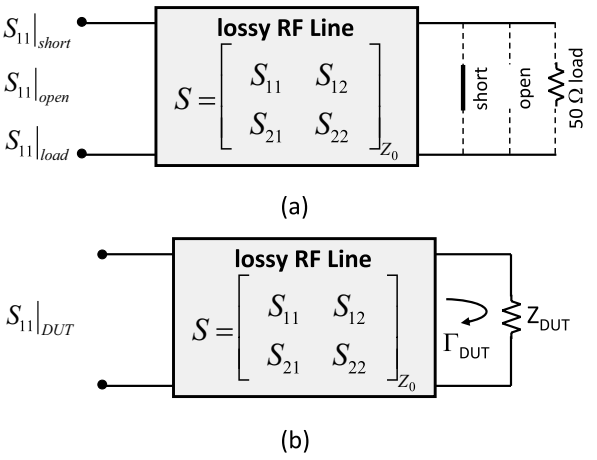


both magnitude and phase) at the input port of the lossy line corresponding to three separate termination conditions, as illustrated in Figure 13.8a, we obtain the following set of *S*-parameters, assuming the load is close to the matched condition (where the load reflection is small):

$$S_{11} = S_{11,load},$$

$$S_{21} = \sqrt{\left( \frac{S_{11,load} - S_{11,short} \quad 2S_{11,open} - 2S_{11,load}}{S_{11,open} - S_{11,short}} \right)}, \quad S_{22} = \frac{S_{11,open} - 2S_{11,load} + S_{11,short}}{S_{11,open} - S_{11,short}}$$

**(13.21)**

A fourth measurement involving the DUT is performed in the exact same manner as that for the calibrated standard loads as shown in Figure 13.8b. This measurement provides information about the reflection loss as seen by the source, but it also provides information about what the lossy line sees at the load end of the line. Let us assume that the line is terminated with a device having input impedance $Z_{DUT}$ and that the wave parameter made at the input of the line is $S_{11,DUT}$. In this case, the reflection loss seen by the source is simply

$$\text{RL} = -20 \cdot \log_{10} \left| S_{11,DUT} \right| \tag{13.22}$$

and, equivalently, the mismatch loss ML can be computed from

$$\text{ML} = -10 \cdot \log_{10} \left( 1 - \left| S_{11,DUT} \right|^2 \right) \tag{13.23}$$

The load reflection coefficient $\Gamma_{DUT}$ corresponding to the impedance seen looking into the load at the interface of the line and load can be computed according to

$$\Gamma_{DUT} = \frac{\left(S_{11,DUT} - S_{11,load}\right)}{S_{21} \cdot S_{12} + S_{22} \cdot \left(S_{11,DUT} - S_{11,load}\right)} \tag{13.24}$$

This, in turn, implies that the equivalent impedance seen by the lossy RF line toward the load side is

$$Z_{DUT} = Z_0 \left(\frac{1+\Gamma_{DUT}}{1-\Gamma_{DUT}}\right)\Omega \tag{13.25}$$

where $Z_0$ is generally assumed to be equal to 50 Ω.

Now that the lossy RF line has been fully characterized, we can quantify the input operating gain, $G_{o,IN}$, through a network analysis in terms of the *S*-parameters of the line, as well as the reflection coefficient at the DUT interface $G_{o,IN}$, to find

$$G_o = \frac{\left(1-\left|\Gamma_{DUT}\right|^2\right)}{\left|1-S_{22} \cdot \Gamma_{DUT}\right|^2} \left|S_{12} \cdot S_{21}\right| \tag{13.26}$$

The operating losses OL would then be computed from this operating gain according to Eq. (13.17).

Returning to the test setup shown in Figure 13.6, we can make use of the above theory and determine the operating loss of the input and output signal paths. In the case of the input path, we would insert the calibration standards into the DUT socket and perform the corresponding $S_{11}$ measurements. Collectively, the *S*-parameters of the input signal path would then be determined through application of Eq. (13.21). Next, the $S_{11}$ parameter corresponding to the line loaded with the input port of the DUT would be measured. Finally, we can put all the measurements together to arrive at the input path operating gain as

$$G_{o,IN} = \frac{\left(1-\left|\Gamma_{IN,DUT}\right|^2\right)}{\left|1-S_{22}^{IN} \cdot \Gamma_{IN,DUT}\right|^2} \left|S_{12}^{IN} \cdot S_{21}^{IN}\right| \tag{13.27}$$

where

$$\Gamma_{IN,DUT} = \frac{\left(S_{11,DUT}^{IN} - S_{11,load}^{IN}\right)}{S_{12}^{IN} \cdot S_{21}^{IN} + S_{22}^{IN} \cdot \left(S_{11,DUT}^{IN} - S_{11,load}^{IN}\right)} \tag{13.28}$$

Here we make use of the superscript *IN* as a reference to the specific *S*-parameters related to the input signal path. These superscripts are only used here to distinguish from the parameters related to the output signal path with the superscript OUT. Often, we will simply drop their use from our notation if their meaning is clear from the context (such as in Example 13.3).

In the case of the output signal path, the approach is very similar. The exception is that the test signal is driven into the output port of the load board where the meter would normally be connected. While the flow of power is opposite to that which the signal path normally sees, this prevents no difficulty to the characterization result, since the transmission line is reciprocal in nature. Also, we should note that output port of the DUT is used to load the line instead of the DUT input port. The DUT must be biased under normal operating conditions during this test. The output signal path gain would then be found from

$$G_{o,OUT} = \frac{\left(1-\left|\Gamma_{OUT,DUT}\right|^2\right)}{\left|1-S_{22}^{OUT}\cdot\Gamma_{OUT,DUT}\right|^2}\left|S_{12}^{OUT}\cdot S_{21}^{OUT}\right| \tag{13.29}$$

where

$$\Gamma_{OUT,DUT} = \frac{\left(S_{11,DUT}^{OUT}-S_{11,load}^{OUT}\right)}{S_{12}^{OUT}\cdot S_{21}^{OUT}+S_{22}^{OUT}\cdot\left(S_{11,DUT}^{OUT}-S_{11,load}^{OUT}\right)} \tag{13.30}$$

The in-socket calibration method of computing operating losses is more advantageous than the method based on estimated mismatch losses, because it is a true measurement of power loss. Moreover, this method includes any power loss due to mismatches in the signal path, any variations in the operating conditions of the device, and any dissipative loss associated with the board traces and matching components. Finally, the *S*-parameter-based measurement approach is not subject to the measurement uncertainty. This is a result of using both magnitude and phase information in all calculations.

## EXAMPLE 13.3

What is the operating loss associated with the input side of the interface board shown in Figure 13.6, if the following measurements at the input port to the board were obtained using the in-socket calibration method, together with a DUT measurement:

$$S_{11,DUT} = -0.2 + j0.2, \quad S_{11,open} = -0.9 - j0.1,$$

$$S_{11,short} = 0.8 + j0.1, \quad S_{11,load} = -0.7 - j0.1$$

**Solution:**

The input side of the interface board shown in Figure 13.6 includes a lossy trace, an RF connector, and a socket for the DUT. Since the $S_{11}$ port measurements include the effects of all three components in their result, the network diagram shown in Figure 13.7d correctly models this situation. We can then use the theory above to determine the operating loss of this interface board.

Using the above measured data, together with the *S*-parameter formulae seen listed in Eq. (13.21), we compute

$$\begin{aligned} S_{22} &= \frac{S_{11,open}-2S_{11,load}+S_{11,short}}{S_{11,open}-S_{11,short}} \\ &= \frac{(-0.9-j0.1)-2(-0.7-j0.1)+(0.8+j0.1)}{(-0.9-j0.1)-(0.8+j0.1)} \\ &= -0.7679 - j0.0273 \end{aligned}$$

and

$$\begin{aligned} S_{12} = S_{21} &= \sqrt{\left(S_{11,load}-S_{11,short}\right)\cdot\left(\frac{2S_{11,open}-2S_{11,load}}{S_{11,open}-S_{11,short}}\right)} \\ &= \sqrt{\left[(-0.7-j0.1)-(0.8+j0.1)\right]\cdot\left[\frac{2(-0.9-j0.1)-2(-0.7-j0.1)}{(-0.9-0.1)-(0.8+j0.1)}\right]} \\ &= 0.0046 - j0.5946 \end{aligned}$$

Next, using Eq. (13.27), we solve for the reflection coefficient at the input terminals of the DUT as

$$\begin{aligned}\Gamma_{IN,DUT} &= \frac{\left(S_{11,DUT} - S_{11,load}\right)}{S_{21}\cdot S_{12} + S_{22}\cdot\left(S_{11,DUT} - S_{11,load}\right)} \\ &= \frac{(-0.2 + j0.2) - (-0.7 - j0.1)}{(0.0046 - j0.5946)(0.0046 - j0.5946) + (-0.7679 - j0.0273)\left[(-0.2 + j0.2) - (-0.7 - j0.1)\right]} \\ &= -0.740 - j0.158\end{aligned}$$

Finally, we compute the operating loss using Eqs. (13.27) and (13.17) as follows:

$$\begin{aligned}G_{o,IN} &= \frac{\left(1 - |\Gamma_{DUT}|^2\right)}{|1 - S_{22}\cdot\Gamma_{DUT}|^2}|S_{12}\cdot S_{21}| \\ &= \frac{\left(1 - |-0.740 - j0.158|^2\right)|(0.0046 - j0.5946)\cdot(0.0046 - j0.5946)|}{|1 - (-0.7679 - j0.0273)\cdot(-0.740 - j0.158)|^2} \\ &= 0.719\end{aligned}$$

and

$$\mathrm{OL}|_{\mathrm{dB}} = -10\cdot\log_{10}\left(G_{o,IN}\right) = -10\cdot\log_{10}(0.719) = 1.434\ \mathrm{dB}$$

The operating loss of the input RF line is then found to be 1.434 dB. It is interesting to note that the device is operating with an input impedance given by

$$\begin{aligned}Z_{DUT} &= \left(\frac{1 + \Gamma_{DUT}}{1 - \Gamma_{DUT}}\right)\times 50\ \Omega \\ &= \left[\frac{1 + (-0.740 - j0.158)}{1 - (-0.740 - j0.158)}\right]\times 50\ \Omega \\ &= 7.01 - j5.187\ \Omega\end{aligned}$$

Clearly the input impedance to the device is significantly different from the ideal situation of 50 Ω.

### 13.1.3 Scalar Power Measures Versus Time

A common measurement for dynamic systems is measure of how signal power varies over time. Typical examples are the power droop when turning on an amplifier or the settling time of a transceiver. Another common measurement is one that observes how the signal frequency changes over time, such as that related to the settling time of a VCO controlled by a PLL. Both measurements are executed in the same way by sampling of the RF power signal; the difference is in the analysis of the captured data.

To measure the time-dependent power such as that shown in Figure 13.9, it will be necessary to synchronize the digitizer with the device by utilizing the trigger bus of the test system and start digitizing the power at a known time point. This might be set within a digital pattern controlling the state of the device. The captured time signal can be processed to calculate the envelope using the ATE DSP or PC algorithm. The envelope is representative of the RF power over time, which can be extracted by calculating the peak power per period of the RF sinusoidal signal.

## Exercises

**13.3.** A gain test was performed on a DUT and found to be 8.76 dB. The DUT is connected to an ATE through an interface board with an operating loss of 0.9 dB. What is the actual gain of the device?

ANS. 9.66 dB.

**13.4.** A gain test was performed on a DUT using an ATE with an interface board. The gain was found to be 8.76 dB. If the source, the meter, and the input and output ports of the DUT have return losses of 10, 12, 20, and 9 dB, respectively, and the traces introduce losses totaling 0.35 dB, what is actual gain of the DUT?

ANS. $9.39\ \text{dB} \le G_A' \le 11.49\ \text{dB}$.

**13.5.** What is the operating loss associated with the output side of an interface board shown in Figure 13.6, if the following measurements at the output port of the board were obtained using the in-socket calibration method, together with a single DUT measurement:

$S_{11,DUT} = 0.1 + j0.2$, $S_{11,open} = -0.8 - j0.2$,
$S_{11,short} = 0.9 + j0.2$, and $S_{11,load} = -0.4 - j0.2$.

ANS. 1.67 dB.

**13.6.** For the conditions specified in Exercise 13.3, what is the output impedance of the DUT?

ANS. $9.0 - j7.8\ \Omega$.

**Figure 13.9.** Time-dependent power with power mask.

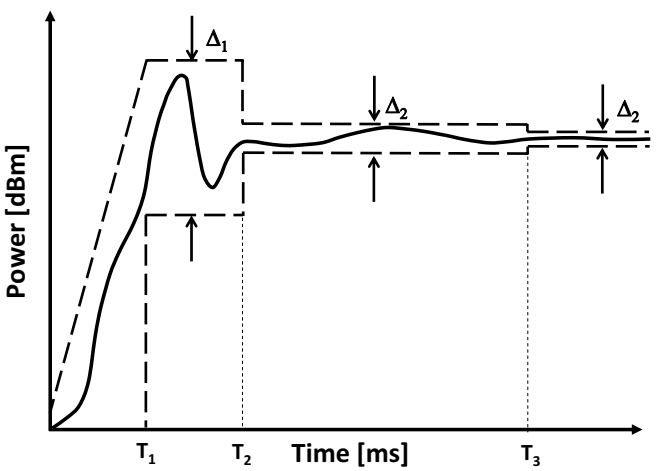

Similar to the measurement of the power over time, the measurement of the frequency components of a signal over time can also be captured. This is required when measuring the lock-in time of a VCO. Instead of calculating the envelope, the signal needs to be FM demodulated in the ATE DSP, where the demodulated signal will be the frequency envelope of the signal.

### 13.1.4 Intermodulation Measurement

The *n*th-order intercept point is a single figure of merit describing the nonlinear performance of an RF system or DUT. The intercept point is a purely mathematical concept and does not correspond to any practically occurring physical power level. In fact, in many cases, it exceeds the damage threshold of the device.

Intermodulation or intermodulation distortion (IMD) is the result of two or more signals of different frequencies being mixed together forming additional signals at frequencies that are not, in general, at harmonic frequencies of each other. Intermodulation is caused by the nonlinear behavior of the RF system.

The power output of a device or system can be expressed in terms of the input power level as a power series representation as follows:

$$P_{out} = a_0 + a_1 P_{in} + a_2 P_{in}^2 + a_3 P_{in}^3 + \cdots + a_n P_{in}^n \tag{13.31}$$

For a two-tone unit amplitude signal with frequencies $\omega_1$ and $\omega_2$, described as

$$P_{in} = \cos(\omega_1 t) + \cos(\omega_2 t) \tag{13.32}$$

the output signal of the device or system can be expressed as

$$\begin{aligned} P_{out} = {} & a_0 + a_1\left[\cos(\omega_1 t) + \cos(\omega_2 t)\right] + a_2\left[\cos(\omega_1 t) + \cos(\omega_2 t)\right]^2 \\ & + a_3\left[\cos(\omega_1 t) + \cos(\omega_2 t)\right]^3 + \cdots + a_n\left[\cos(\omega_1 t) + \cos(\omega_2 t)\right]^n \end{aligned} \tag{13.33}$$

Equation (13.33) can be rewritten as

$$\begin{aligned} P_{out} = {} & a_0 + a_1\left\{\cos(\omega_1 t) + \cos(\omega_2 t)\right\} \\ & + a_2\left\{\cos^2(\omega_1 t) + \cos^2(\omega_2 t) + 2\cos(\omega_1 t)\cdot\cos(\omega_2 t)\right\} \\ & + a_3\left\{\cos^3(\omega_1 t) + \cos^3(\omega_2 t) + 3\cos^2(\omega_1 t)\cdot\cos(\omega_2 t) + 3\cos(\omega_1 t)\cdot\cos^2(\omega_2 t)\right\} + \cdots \end{aligned} \tag{13.34}$$

By using the trigonometric identities

$$\cos(x)\cdot\cos(y) = \frac{1}{2}\left\{\cos(x-y) + \cos(x+y)\right\}$$

$$\cos^2(x) = \frac{1}{2}\left\{1 + \cos(2x)\right\}$$

$$\cos^3(x) = \frac{1}{4}\left\{3\cos(x) + \cos(3x)\right\}$$

and

$$\cos(x)\cdot\cos^2(y) = \frac{1}{4}\left[2\cos(x) + \cos(2y - x) + \cos(x + 2y)\right]$$

Equation (13.34) can be further written in terms of cosine functions of first order. For instance, the third-order term of Eq. (13.34) can be written (ignoring the leading coefficient) as follows

$$P_3 \propto \cos(\omega_1 t)+\cos(\omega_2 t)+\cos(3\omega_1 t)+\cos(3\omega_2 t)+\cos(2\omega_1 t-\omega_2 t)+\cos(2\omega_1 t+\omega_2 t) \\ +\cos(2\omega_2 t-\omega_1 t)+\cos(2\omega_2 t+\omega_1 t) \quad \textbf{(13.35)}$$

The above equation reveals some important system behavior. Here we see that the third-order term contains additional signals other than the inputs at frequencies at $3\omega_1$, $3\omega_2$, $2\omega_2 + \omega_1$, $2\omega_1 + \omega_2$, $2\omega_1 - \omega_2$, and $2\omega_2 - \omega_1$. A diagram depicting the third order distortion products, including its 2nd-order harmonics, is shown in Figure 13.10. The first four terms are relatively far away from the input frequencies ($\omega_1$ and $\omega_2$) and can easily be filtered out. However, the latter two terms, and, are very close to the two input frequencies. These two terms cannot be easily filtered out and are commonly referred to as the third-order intermodulation products. It is important to note that the intermodulation products will increase with increasing input power faster than the tones at the fundamental input frequencies. In dBm units, the third-order intermodulation signal will increase in power three times as fast as the power associated with the fundamental signals.

**Figure 13.10.** Frequency spectrum of a 2-tone signal driving a non-linear system.

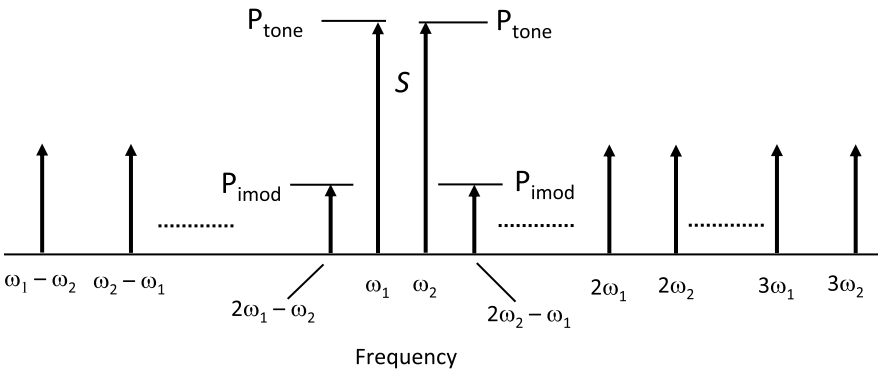


**Figure 13.11.** Illustration of the Third Order Intercept Point (IP3).

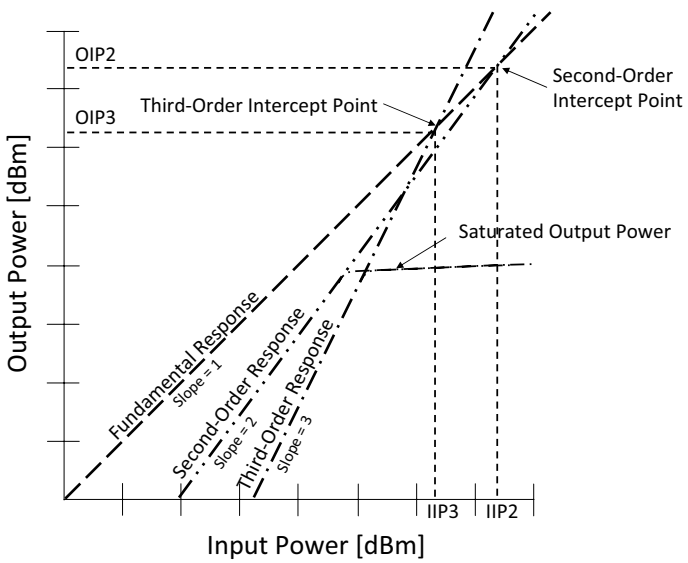

This is evident in the plot of a breakdown of the output power as a function of the input power shown in Figure 13.11. Here the powers of the fundamental, second-order and third-order intermodulation terms are plotted as a function of the input power level. We also noticed in this plot that the second-order and third-order response intersects with the fundamental response, at least the straight-line representation, at two separate points. In the case of the second-order response, the intersection point is called the second-order intercept (IP2) and, likewise, for the third-order response it is called the third-order intercept point (IP3). Since any point in a two-dimensional Cartesian plane is represented by two values, here the intercept points are presented by the input-referred and output referred value. In the case of the third-order intercept, we refer to the input-referred value as IIP3 and the output-referred value as OIP3. Intercept points are commonly found on the data sheet of an RF device.

To measure say the third-order intercept point, it is necessary to source a two-tone signal with equal tone powers to the RF system or DUT. The frequency spacing between each tone should be selected such that the third-order intermodulation distortion products are within the nominal bandwidth of the system or DUT and do not get filtered or attenuated other than that experienced by the input tones. The power level needs to be below the compression point of the system or DUT, but also as high as possible so that the intermodulation distortion products are well above the measurement noise floor. The critical step in measuring the IP3 is to measure the power level of the intermodulation distortion products, which can be very low in comparison to the strong input tones. Some optimization of the maximum expected power level, the measurement bandwidth, and the sample rate and size is required for a given IP3 test. Since the measurement path of the ATE will have its own nonlinear performance, it is imperative to keep the system distortion products smaller than those of the DUT by staying within the linear region of the system. Distortions from two separate sources, in general, cannot be separated from one another.

Assuming that the power of the fundamental tones at the output of the device is $P_{OUT}$, and the power associated with the in-band third-order tones is $P_{imod}$, then the IIP3 relative to the OIP3 is found from

$$\text{IIP3}\big|_{\text{dBm}} = \text{OIP3}\big|_{\text{dBm}} - \text{Gain}\big|_{\text{dB}} \tag{13.36}$$

where OIP3 is given by

$$\text{OIP3}\big|_{\text{dBm}} = P_{tone}\big|_{\text{dBm}} + \frac{1}{2}\left(P_{tone}\big|_{\text{dBm}} - P_{imod}\big|_{\text{dBm}}\right) \tag{13.37}$$

Theoretically, the two fundamental input power levels will be equal to one another, and the two intermodulation distortion products' power levels will also be equal. In general, this assumption is usually valid, so either tone could be taken to calculate the intercept point. However, in some cases, the test equipment will result in a measurement of different levels for these tones. For these cases, an investigation is required to find the root cause, which might be the calibration or a filter of the ATE. One other root cause could be that the fundamental tones are amplified differently in the DUT, causing an unequal power level of the tones. In this case, it is a common practice to measure all four tones and calculate the worst-case intercept point value (i.e., smallest IIP3 or OIP3). We should also mention that the gain of the device is found as the ratio of the output fundamental power to the input fundamental power.

In much the same manner, the second-order intercept point, IP2, is obtained by sourcing a two-tone signal to the RF system or DUT and measuring the second-order intermodulation distortion products. The second-order distortion products will have a signal at the following frequencies: $DC$, $2\omega_1$, $2\omega_2$, $\omega_1 + \omega_2$, $\omega_1 - \omega_2$, and $\omega_2 - \omega_1$. Assuming that the power of the fundamental tones at the output of the device is $P_{OUT}$, and the power associated with the in-band second-order tones is $P_{imod}$, then the OIP2 is found from

$$\text{OIP2}\big|_{\text{dBm}} = 2 \cdot P_{tone}\big|_{\text{dBm}} - P_{imod}\big|_{\text{dBm}} \tag{13.38}$$

and the input referred second-order intercept point *IIP2* is found from

$$\text{IIP2}\big|_{\text{dBm}} = \text{OIP2}\big|_{\text{dBm}} - \text{Gain}\big|_{\text{dB}} \tag{13.39}$$

The following three examples will help illustrate the application of these formulas to several different situations.

## EXAMPLE 13.4

The intermodulation of an amplifier with a gain of 20 dB is measured. The intermodulation distortion measurements are made at a 15 dBm output-power level per fundamental tone. The intermodulation distortion products power level is at –55 dBm per tone. What is the third order intercept point?

**Solution:**
The third order intercept point can be calculated to

$$\text{OIP3}\big|_{\text{dBm}} = 15\ \text{dBm} + \frac{15\ \text{dBm} - (-55\ \text{dBm})}{2} = 50\ \text{dBm}$$

or

$$\text{IIP3}\big|_{\text{dBm}} = \text{OIP3}\big|_{\text{dBm}} - \text{Gain}\big|_{\text{dB}} = 50\ \text{dBm} - 20\ \text{dB} = 30\text{dBm}$$

## EXAMPLE 13.5

When testing the OIP3 of an amplifier with gain of $G$ = 30 dB,we measure the spectrum shown below. What is the output OIP3 and input-referred IIP3?

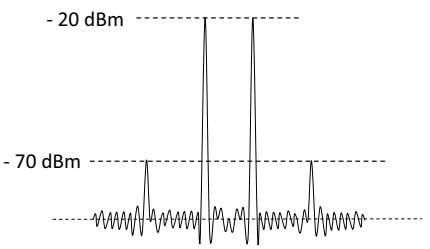


**Solution:**
Using Eq. (13.37), we write

$$\text{OIP3}\big|_{\text{dBm}} = P_{tone}\big|_{\text{dBm}} + \frac{1}{2}\left(P_{tone}\big|_{\text{dBm}} - P_{imod}\big|_{\text{dBm}}\right) = -20\ \text{dBm} + \frac{1}{2}\left[-20\ \text{dBm} - (-70\ \text{dBm})\right] = 5\ \text{dBm}$$

and using Eq. (13.36), we compute

$$\text{IIP3}\big|_{\text{dBm}} = \text{OIP3}\big|_{\text{dBm}} - \text{Gain}\big|_{\text{dB}} = 5\ \text{dBm} - 30\ \text{dB} = -25\ \text{dBm}$$

## EXAMPLE 13.6

The spectrum below has been measured when supplying an amplifier with a –40 dBm per tone two-tone signal. What are the OIP3, IIP3, and the gain of this amplifier?

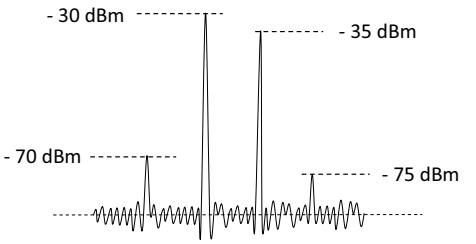


**Solution:**
Because the signal levels are all different, we must determine the worst-case IP3 point. As such, we compute all four possible OIP3 values using Eq. (13.37) as follows:

$$\mathrm{OIP3}_1\big|_{\mathrm{dBm}} = P_{tone1}\big|_{\mathrm{dBm}} + \frac{P_{tone1}\big|_{\mathrm{dBm}} - P_{imod1}\big|_{\mathrm{dBm}}}{2} = -30\ \mathrm{dBm} + \frac{-30\ \mathrm{dBm} - (-70\ \mathrm{dBm})}{2} = -10\ \mathrm{dBm}$$

$$\mathrm{OIP3}_2\big|_{\mathrm{dBm}} = P_{tone2}\big|_{\mathrm{dBm}} + \frac{P_{tone2}\big|_{\mathrm{dBm}} - P_{imod2}\big|_{\mathrm{dBm}}}{2} = -35\ \mathrm{dBm} + \frac{-35\ \mathrm{dBm} - (-75\ \mathrm{dBm})}{2} = -15\ \mathrm{dBm}$$

$$\mathrm{OIP3}_3\big|_{\mathrm{dBm}} = P_{tone2}\big|_{\mathrm{dBm}} + \frac{P_{tone2}\big|_{\mathrm{dBm}} - P_{imod1}\big|_{\mathrm{dBm}}}{2} = -35\ \mathrm{dBm} + \frac{-35\ \mathrm{dBm} - (-70\ \mathrm{dBm})}{2} = -17.5\ \mathrm{dBm}$$

$$\mathrm{OIP3}_4\big|_{\mathrm{dBm}} = P_{tone1}\big|_{\mathrm{dBm}} + \frac{P_{tone1}\big|_{\mathrm{dBm}} - P_{imod2}\big|_{\mathrm{dBm}}}{2} = -30\ \mathrm{dBm} + \frac{-30\ \mathrm{dBm} - (-75\ \mathrm{dBm})}{2} = -7.5\ \mathrm{dBm}$$

Because the smallest or lowest OIP3 value represents the worst-case value, we note

$$\mathrm{OIP3}_{w/c}\big|_{\mathrm{dBm}} = -17.5\ \mathrm{dBm}$$

Next, the gain of the amplifier is found as the ratio of the output tone power to the input power level (or, equivalently, the difference in dBm). Since there are two different output levels corresponding to the fundamental frequencies, we compute the gain of each tone as

$$G_1\big|_{\mathrm{dB}} = -30\ \mathrm{dBm} - (-40\ \mathrm{dBm}) = 10\ \mathrm{dB}$$
$$G_2\big|_{\mathrm{dB}} = -35\ \mathrm{dBm} - (-40\ \mathrm{dBm}) = 5\ \mathrm{dB}$$

Finally, we compute the worst-case IIP3 using Eq. (13.36) as

$$\mathrm{IIP3}_1\big|_{\mathrm{dBm}} = \mathrm{OIP3}_{w/c}\big|_{\mathrm{dBm}} - G_1\big|_{\mathrm{dB}} = -17.5\ \mathrm{dBm} - 10\ \mathrm{dB} = -27.5\ \mathrm{dBm}$$
$$\mathrm{IIP3}_2\big|_{\mathrm{dBm}} = \mathrm{OIP3}_{w/c}\big|_{\mathrm{dBm}} - G_2\big|_{\mathrm{dB}} = -17.5\ \mathrm{dBm} - 5\ \mathrm{dB} = -22.5\ \mathrm{dBm}$$

The worst-case IIP3 (lowest value) is therefore

$$\mathrm{IIP3}_{w/c}\big|_{\mathrm{dBm}} = -27.5\ \mathrm{dBm}$$

**Exercises**

**13.7.** The intermodulation of an amplifier with a gain of 15 dB is measured. The intermodulation distortion measurements are made at a –21-dBm output-power level per fundamental tone. The intermodulation distortion products power level is at –73 dBm per tone. What is the second-order intercept point?

ANS. IIP2 = 16 dBm, OIP2 = 31 dBm.

**13.8.** The spectrum below has been measured when supplying an amplifier with a –30 dBm per tone two-tone signal. What is the OIP3, the IIP3, and the gain of this amplifier?

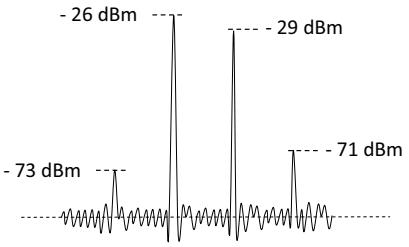


ANS. IIP3 = –12 dBm, OIP3 = –8 dBm, $G$ = 4 dB (all worst-case).

## 13.1.5 Compression Point Measurement

The dynamic range of an amplifier is determined by its noise figure and 1-dB compression point. In multicarrier applications, the third-order intercept point also plays a role in its dynamic range. The compression point, denoted by the parameter P1dB, is the input power level at which the gain will deviate 1 dB from its small signal gain as illustrated in Figure 13.12. The value of 1 dB is commonly used but any other value could be specified, like, for instance, a 0.1-dB compression point. In this subsection, we will describe four different methods to test for the 1-dB compression point of a DUT. All four methods are based on the same approach: Sweep the input power level, calculate the gain of the device, and then decide where the 1-dB compression point is located.

### *Go–No-Go Method*

The exact 1-dB compression point (P1dB) is not measured with the Go–No-Go method. This method is more useful for production tests, which have a pass–fail criterion. The gain of the device is tested well below the P1dB, and a second gain is tested at the power level specified for the device in the data sheet as the minimum P1dB. If the gain difference between the two measurements is less than 1 dB, the device will pass the test, because the actual P1dB point will occur at a higher input level than that specified in the data sheet. Since the measurement error for both gain tests can add up, it is necessary to minimize the measurement error by optimizing the ATE setting (e.g., establish the optimum power level), as well average the nominal small signal gain measurement over multiple runs to improve its measurement accuracy.

### *Binary Search Method*

Another method for measuring the P1dB is to vary the input power and to apply a binary search routine (see further details in Chapter 3, Section 3.11) such as that illustrated in Figure 13.13 for an eight-step search. Since the gain is nonlinear around the P1dB, it will take a couple of iterations to be within a predefined band around the actual P1dB. Nonetheless, the search is quite fast when compared to a step search. A binary search will not work on multiple devices connected in parallel to a single source

**Figure 13.12.** Go–no-go method to test for P1dB specification.

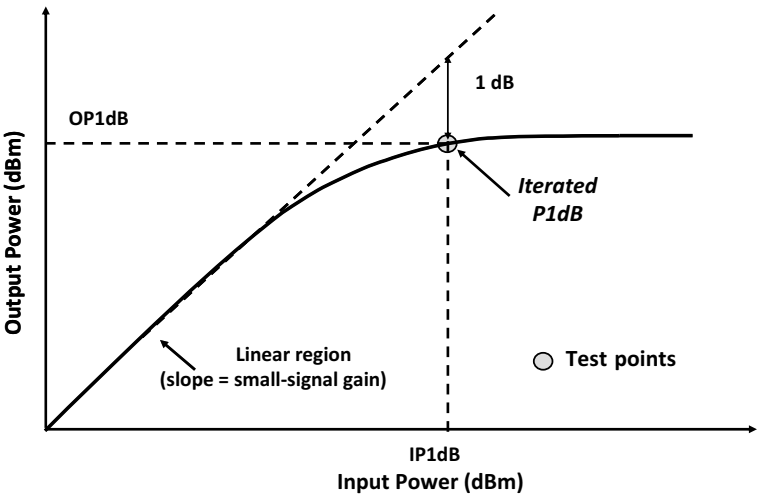


**Figure 13.13.** Binary search method to measure the P1dB.

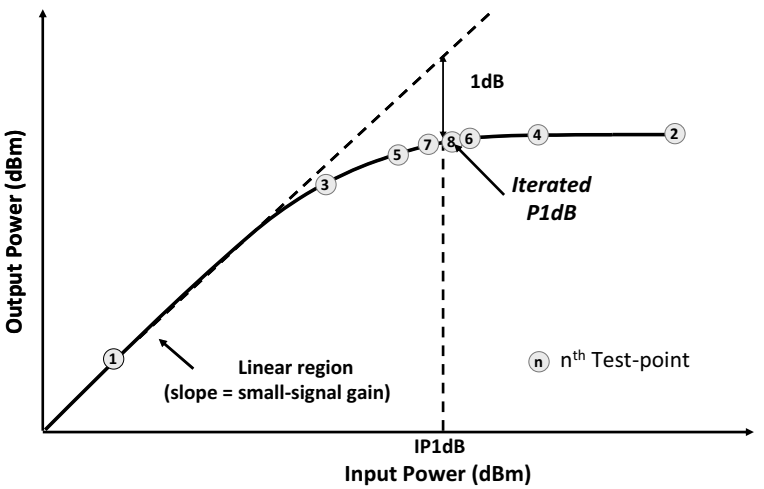


for the simple reason that it operates by adjusting the input power level such that a desired output is achieved. Since multiple devices have multiple outputs, the algorithm simply does not apply. Instead, one must resort to searching the P1dB one device at a time. In addition, because the search process is different for each device, the number of iterations required can also vary. This, in turn, can create complications with the data analysis tools associated with some testers. Also, one must be aware that the source and measurement error can accumulate and cause the search process to go longer than expected. Even more seriously is the potential for the search process to oscillate about a region that includes the P1dB. It is therefore important that the search algorithm take the instrument errors into account.

### *Interpolation Method*

With the interpolation method, a predefined number of gain tests are taken over a range of input power levels, which includes the input power level corresponding to the expected 1-dB compression point. Such a situation is depicted in Figure 13.14. The power levels are usually selected with

**Figure 13.14.** Interpolation method applied to gain vs. input level to determine the P1dB.

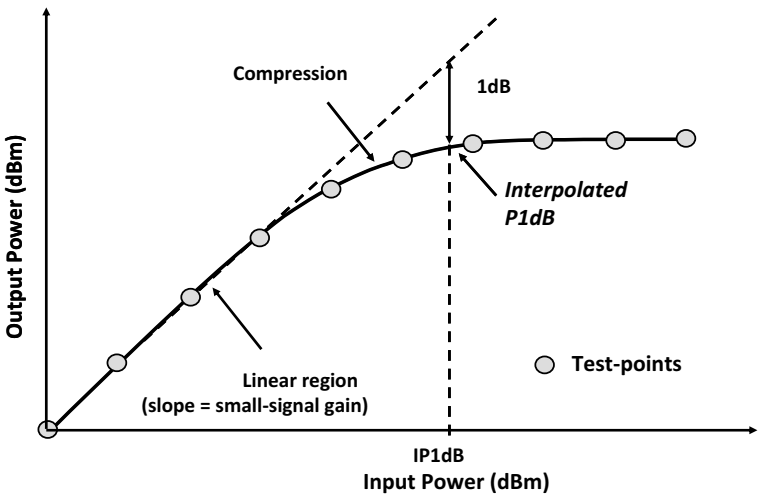


a constant power difference (e.g., 2 dB). These measurements can be analyzed in several ways to find the P1dB of the DUT. Two methods are described below:

1. The actual gain curve can be reconstructed with a high-order polynomial approximation such as using the Lagrange's interpolation method. For an $\Psi$-point data set, $[(P_{in,1},G_1),\ldots,(P_{in,k},G_k),\ldots,(P_{in,\Psi},G_\Psi)]$, one can write the interpolation equation for the gain at any power level for an input power range defined between $P_{in,1}$ and $P_{in,\Psi}$ as

$$G\left(P_{in}\right)=\sum_{i=1}^{\Psi}L\left(i,P_{in}\right)G_i \tag{13.40}$$

where

$$L\left(i,P_{in}\right)=\frac{\left(P_{in}-P_{in,1}\right)\ldots\left(P_{in}-P_{in,i-1}\right)\left(P_{in}-P_{in,i+1}\right)\ldots\left(P_{in}-P_{in,\Psi}\right)}{\left(P_{in,i}-P_{in,1}\right)\ldots\left(P_{in,i}-P_{in,i-1}\right)\left(P_{in,i}-P_{in,i+1}\right)\ldots\left(P_{in,i}-P_{in,\Psi}\right)}$$

Once the model of the power gain is formulated in terms of the input power level, the P1dB point can be determined through some mathematical root finding procedure such as those described earlier in Chapter 3, Section 3.11. Specifically, we solve for the P1dB from the expression

$$G\left(\text{P1dB}\right)=G_{nom}-1 \tag{13.41}$$

where $G_{nom}$ is the nominal small-signal gain found under low power conditions. Since the search process is performed in software on a mathematical function rather than through a control loop involving the instruments interacting with the DUT, this approach can be a very time efficient. We leave the details of this procedure to Exercises 13.9 and 13.10.

2. A search routine can be implemented in the test program to find the closest two power levels that bound the 1-dB compression point. Let's say that this occurs between the ($k$–1)th and kth input power step. Using with the nominal small-signal gain $G_{nom}$ found in a separate measurement, together with the gains corresponding to the ($k$–1)th and $k$th step, denoted $G_{k-1}$ and $G_k$, together with the two corresponding input power levels, $P_{in,k-1}$ and $P_{in,k}$, we can estimate the 1-dB compression point from the following straight-line approximation:

$$\text{P1dB}_{est}=P_{in,k-1}+\left[\frac{G_{k-1}-G_{nom}+1}{G_{k-1}-G_k}\right]\left[P_{in,k}-P_{in,k-1}\right] \tag{13.42}$$

**Figure 13.15.** Interpolation between two points that encompass the 1-dB compression point.

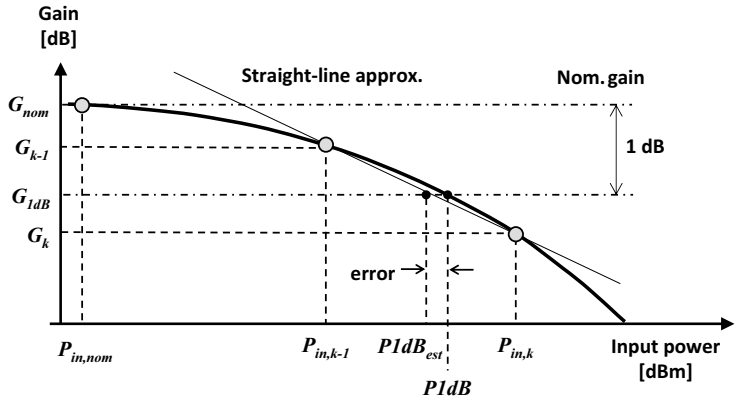


**Figure 13.16.** P1dB measurement with a single data capture using a modulated input signal: (a) a segmented waveform, (b) a saw-tooth power waveform for continuous power variation.

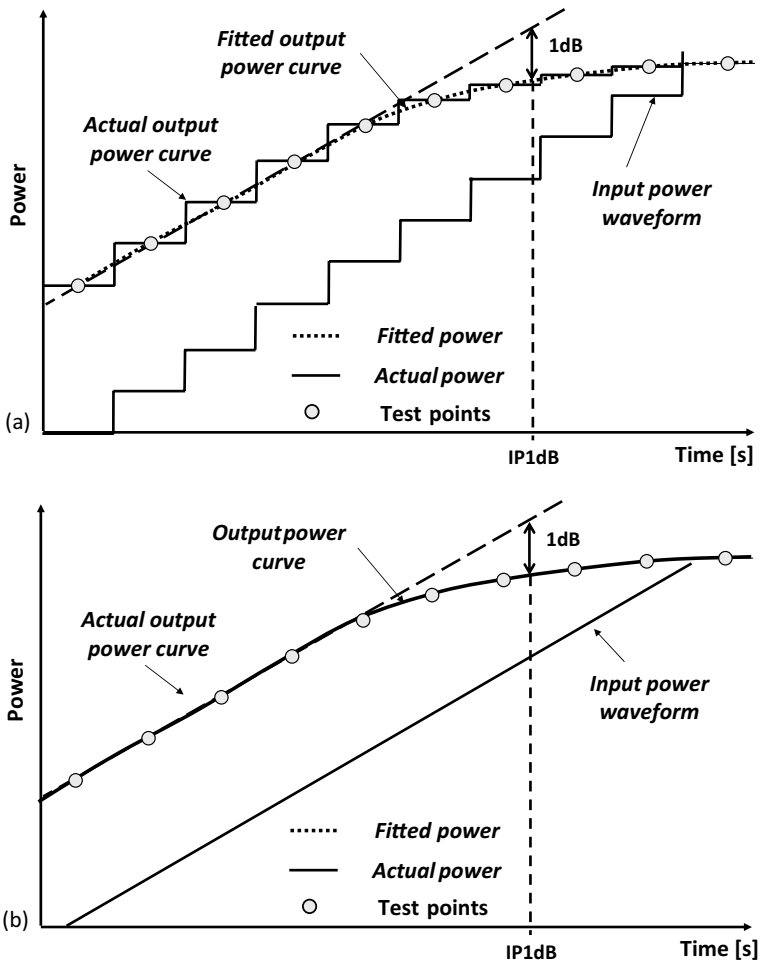

Figure 13.15 illustrates the idea behind this approximation. The inherent error of this method is small for reasonable input power step size.

The advantage of either of these two interpolation methods is that the individual gain measurements across a lot of devices can be compared, since all are taken under the same input conditions. This information can be quite useful during the test debug phase.

### *Modulation Method*

The fourth method is similar to the interpolation method just described, except that the gain is not measured at individual input power levels using a continuous-wave stimulus, but rather with a modulated input signal containing the various power levels over different sections of the modulated waveform, such as that shown in Figure 13.16a. When driving the DUT with this waveform and capturing the output power over time, the individual power levels can be extracted and calculated from a single

## EXAMPLE 13.7

The measurements below are taken on a PA to test the P1dB point. The small signal gain had been measured previously and found to be equal to 19.60 dB. Estimate the P1dB point with the given data (which contain a realistic repeatability and accuracy error).

| Step | Input [dBm] | Gain [db] |
|---|---|---|
| 1 | 0 | 19.566 |
| 2 | 1 | 19.405 |
| 3 | 2 | 19.237 |
| 4 | 3 | 19.027 |
| 5 | 4 | 18.653 |
| 6 | 5 | 18.352 |
| 7 | 6 | 17.875 |
| 8 | 7 | 17.423 |
| 9 | 8 | 16.831 |
| 10 | 9 | 16.313 |

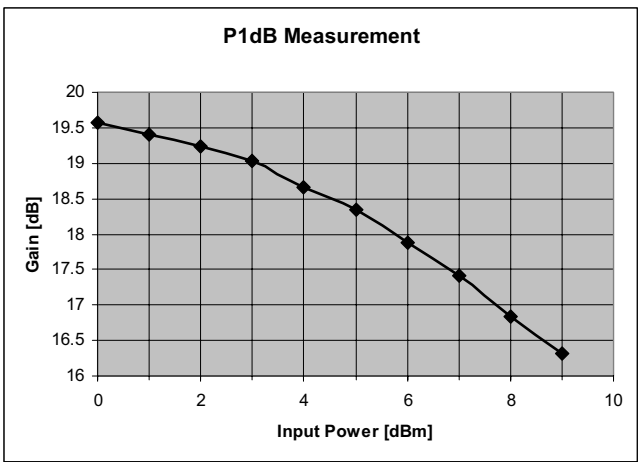


**Solution:**

With a nominal gain of 19.60 dB, the 1-dB compression point occurs at 18.60 dB. Therefore, we observe from the tabulated data that the 1-dB compression point occurs between an input power level of 4 and 5 dBm (step 5 and 6). Using Eq. (13.42), we get

$$\begin{aligned} \text{P1dB}_{est} &= P_{in,5} + \left[\frac{G_5 - G_{nom} + 1}{G_5 - G_6}\right]\left[P_{in,6} - P_{in,5}\right] \\ &= 4\ \text{dBm} + \left[\frac{18.653\ \text{dB} - 19.6\ \text{dB} + 1}{18.653\ \text{dB} - 18.352\ \text{dB}}\right]\left[5\ \text{dBm} - 4\ \text{dBm}\right] \\ &= 4.176\ \text{dBm} \end{aligned}$$

Therefore we estimate the 1-dB compression point at 4.176 dBm.

captured array. These individual gain values can be processed in the same way as was done with the interpolation method. Instead of setting up the waveform with separate power levels, the power level can be steadily increased in a sawtooth-like manner, such as that shown in Figure 13.16b. The reconstructed gain curve can then be used to compute the 1-dB compression point.

The advantage of the modulated method is that the 1-dB compression point can be accurately measured with a single data capture. The data can be analyzed in the ATE DSP, or as a background process while the ATE is executing another test. The disadvantage is that the requirement to create a complex input waveform and that the ATE needs to have a source with modulation capability. Another advantage of sourcing a modulated signal is the high relative power accuracy. The reconstruction of the output power curve also minimizes the measurement error by a weighted averaging of the measured power, which can be typically seen as a smooth regression curve.

## 13.2 *S*-PARAMETER MEASUREMENTS

A special application of a power measurement is one that involves capturing the *S*-parameters of a two-port network. With the addition of some hardware in the RF ATE measurement and source path, the magnitude and phase of the incident and reflected wave can be obtained, allowing the calculation of the corresponding *S*-parameters (see Section 12.4). To be able to measure the *S*-parameter, the ATE needs to be capable of separating the incident and the reflected wave of the signals at the source and measurement side of the DUT. This separation can be done with an RF coupler, which is built into most commercial RF ATE. In the following two subsections, we will discuss the principles of the directional coupler, their physical constraints, and the *S*-parameter measurement technique.

### 13.2.1 Principles of a Directional Coupler

A directional coupler is a passive four-port device, which separates the forward and reverse propagating wave. A symbolic representation of a directional coupler is shown in Figure 13.17. A part of the power transmitted from the *input* to the *transmitted* port will be coupled to the *coupled* port, while a part of the power supplied to the transmitted port will be coupled to the *isolated* port.

The directional coupler can be defined as a four-port device with a corresponding set of *S*-parameters (e.g, $S_{11}$, $S_{12}$, $S_{13}$, $S_{14}$, etc.). For a backward wave coupler (a forward wave coupler would have the coupled port 4 next to the transmitted port 2), port 4 is the coupled port, and port 3 is the isolated port as shown in Figure 13.17. Power supplied to port 1 will ideally appear at port 2, and a portion will be coupled to port 4, but no power will be transmitted to port 3. The insertion loss IL of an ideal coupler is the loss of the through line between *input* port 1 and *transmitted* port 2 and can be defined as the ratio of the corresponding powers, that is,

$$\mathrm{IL}\big|_{\mathrm{dB}} = -10\log_{10}\left(\frac{P_2}{P_1}\right) = 10\log_{10}\left(1-\frac{P_4}{P_1}\right) = -20\log_{10}\left|s_{21}\right| \qquad \textbf{(13.43)}$$

**Figure 13.17.** Schematic symbol of a directional coupler as a four-port device.

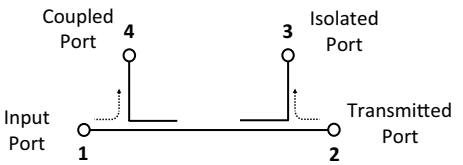

**Exercises**

**13.9.** The minimum P1dB is listed in a device data sheet to be 0 dBm. A gain test is performed for an input of –30 dBm and the gain is found to be 22.3 dB. A second test is performed at 0 dBm and the gain is found to be 21.87 dB. Does this device pass its 1-dB compression point test?

ANS. Yes, as the gain difference is less than 1 dB.

**13.10.** Using the capture data seen listed in Example 13.7, determine the corresponding Lagrange interpolation function. What is the value of this function at an input power level of 3.5 dBm?

$$G\left(P_{in}\big|_{\text{dBm}}\right)\Big|_{\text{dB}} = 19.566 + 2.9160P_{in} - 7.9809P_{in}^2 + 8.0681P_{in}^3 - 4.2441P_{in}^4 + 1.2905P_{in}^5 - 0.2355P_{in}^6 + 0.0254P_{in}^7 - 0.0015P_{in}^8 + 3.71\times10^{-5}P_{in}^9$$

ANS. $G(3.5) = 18.82$ dBm.

**13.11.** Using the binary search method described in Chapter 3, determine the 1-dB compression point for the amplifier described in Exercise 13.9 if the nominal gain is 20.0 dB?

ANS. P1dB = 3.070 dBm.

The coupling factor $C$ is the ratio in decibels of the power that appears at the *coupled* port 4 to that which is applied to the *input* port 1 when all other ports are terminated by an ideal reflection free termination, defined as follows:

$$C\big|_{\text{dB}} = -10\log_{10}\left(\frac{P_4}{P_1}\right) = -20\log_{10}\left|s_{41}\right| \tag{13.44}$$

Real couplers will have some power leaking through to port 3. A quantity used to characterize the power leakage is the isolation factor, $I$. It is defined as the ratio of the power that appears at the isolated port to the input power at port 1,

$$I\big|_{\text{dB}} = -10\log_{10}\left(\frac{P_3}{P_1}\right) = -10\log_{10}\left(\frac{P_4}{P_2}\right) = -20\log_{10}\left|s_{31}\right| = -20\log\left|s_{42}\right| \tag{13.45}$$

The final metric of interest is the directivity factor $D$, which is equal to the difference in decibels between the power that appears at the *coupled* port in the forward direction when the coupled port is terminated to the power that appears at the terminated *isolation* port when driven in the reverse direction (which becomes the coupled port in the reverse direction). It is defined as

$$D\big|_{\text{dB}} = 10\log_{10}\frac{P_4}{P_1} - 10\log_{10}\frac{P_3}{P_1} \tag{13.46}$$

which reduces to

$$D\big|_{\text{dB}} = -10\log_{10}\left(\frac{P_3}{P_4}\right) = -20\log_{10}|s_{34}| \tag{13.47}$$

Practically, the directivity factor should be very high, and this makes it very difficult to measure directly. Instead, using the coupling and isolation definitions of Eq. (13.44) and Eq. (13.45), the directivity factor seen listed in Eq. (13.46) can also be computed as

$$D\big|_{\text{dB}} = I\big|_{\text{dB}} - C\big|_{\text{dB}} \tag{13.48}$$

## 13.2.2 Directional Couplers on an ATE

With the definitions of *S*-parameters provided in Section 4 of Chapter 12, *S*-parameter-type measurements can be made with an ATE so long as it is equipped with directional couplers, sources and some digitizers. Figure 13.18 illustrates the general test set up for extracting the *S*-parameters of a DUT. Two ATE sources are required to drive each side of the DUT. The separation of the incident and reflected wave is done in the hardware with the directional coupler. Each digitizer is used to extract both the magnitude and phase of the voltage signal appearing at the appropriate port of the directional coupler. Even when the ATE has only one digitizer, the incident and reflected waves can still be extracted, albeit each wave $a_1$, $a_2$, $b_1$, and $b_2$, will be extracted sequentially. Of course, it is assumed here that the signals are stationary and their statistics do not change with time.

With the addition of each directional coupler, signal gain from the source to each interface port must be calibrated for its frequency dependencies. This gain dependency must be incorporated into a set of calibration factors, which will be used internally in the ATE to correct the measured magnitude and phase of the captured value. For the situation when the *S*-parameters of the DUT alone is desired, the impact of the load board and socket needs to be measured to calculate an error model. This error model will be used to de-embed the measured *S*-parameter of the load board, socket, and DUT to the DUT-specific *S*-parameter.

The understanding behind the theory behind the *S*-parameter measurement makes this test extremely powerful when describing the performance of an RF DUT.

**Figure 13.18.** Two-port *S*-parameter implementation on an ATE.

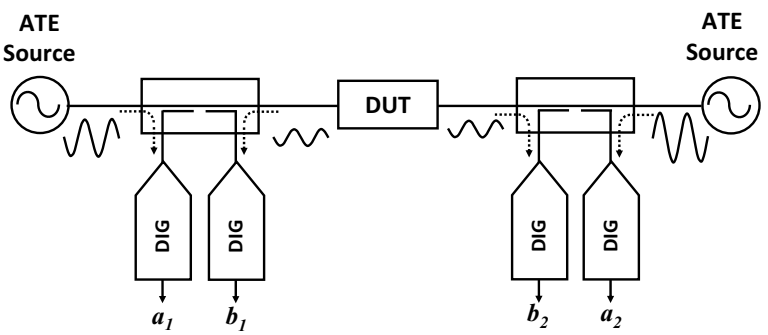

## 13.3 NOISE FIGURE AND NOISE FACTOR

In Section 12.3 we described (a) the theory behind noise and noise figure and (b) its importance as an RF system parameter. In this subsection, we will explain two different techniques for measuring noise figure-specifically, the *Y*-factor method and the cold noise method. While there are additional noise measurement techniques commonly found on a bench setup, such as the 3-dB power increase method, the majority of ATE systems make use of the *Y*-factor and cold-noise methods. We shall therefore limit our discussion here to these two methods.

### 13.3.1 Noise Figure and Noise Factor Definition

It is common to all noise figure tests that thermal noise is considered the dominant component. This simplifies the analysis significantly because thermal noise is also frequency-independent, as outlined in Section 12.3. Recall that the noise factor $F$ of a system or device is defined as the ratio of the signal-to-noise ratio at the input to that found at its output, that is,

$$F = \frac{\mathrm{SNR}_i}{\mathrm{SNR}_o} \tag{13.49}$$

whereby it is assumed that the system or device is operating at a reference temperature of $T_0$. Noise factor is also expressed in terms of decibels, but given the new name of noise figure NF defined as

$$\mathrm{NF} = F\big|_{dB} = 10\log_{10}(F) \tag{13.50}$$

Often 290 K is taken as the reference temperature, because it is declared in one of the IEEE standards, however, the noise figure and noise factor can be defined for any temperature. Since noise is a function of temperature, that is,

$$N = kTB \tag{13.51}$$

device temperature must be declared alongside a noise figure or noise factor in order to compare one device to another.

The noise of an RF system or device can consist of thermal noise or any other noise-generating process, as described in Section 12.3. The individual noise contributions can be added together and regarded as the total noise power. This combined noise power can then be described with a *noise temperature* $T_N$, defined as the temperature generating the equivalent thermal noise $P_N$ in a defined noise bandwidth $B_N$ given by

$$T_N = \frac{P_N}{k\,B_N} \tag{13.52}$$

For systems or devices with the same bandwidth, $B_N$, noise temperature and noise power are proportional to one another, hence noise temperature can be combined in much the same way that noise power is combined-that is, as a linear sum. To see this more clearly, consider the RF system shown in Figure 13.19. Here the noise power associated with the DUT is modeled as a noise component $N_e = kBT_e$ and added to the incoming signal with noise component $N_s = kBT_s$. Moreover, the DUT is now assumed to be noiseless with noise figure $NF = 0$ dB. For a DUT with power gain $G$, the noise appearing at the output can be described as

$$N_o = G(N_S + N_e) \tag{13.53}$$

**Figure 13.19.** Noise temperature to describe the total noise power.

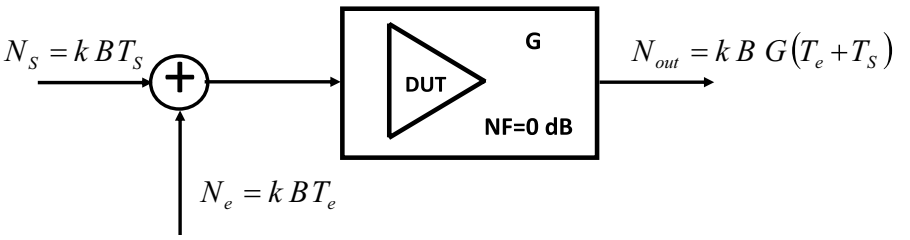


which can be rewritten as

$$N_o = G\left(kBT_S + kBT_e\right) = GkB\left(T_S + T_e\right) \tag{13.54}$$

As is evident from above, the noise at the DUT output is proportional to the linear sum of the noise temperature corresponding to its input and the noise temperature of the DUT itself.

It is worth mentioning that the noise we refer to here is the average noise power over a predefined bandwidth. Moreover, this noise metric does not include any signals like spurious or other unwanted signals like the harmonics associated with the power supply.

To measure the noise figure of a device, a noise source is often used. This source generates a noise power having specific statistical quantities as a function of a DC input voltage. Most of the commercially available noise sources have two defined states, one for a 0-V input and another typically found at a 28-V input. These two states give rise to two distinct noise power levels, referred to as the hot and cold noise levels ($N_{hot}$ and $N_{cold}$) or as the on and off noise levels ($N_{\text{on}}$ and $N_{\text{off}}$). Equivalently, and not surprising, the hot and cold noise levels can be described with two temperatures $T_{hot}$ and $T_{cold}$. It is a common practice to quantify the function of the noise source with the parameter *excess noise ratio* or *ENR* value. The *ENR* value of a noise source describes the noise output of a source compared to the off-state of the noise source, given by

$$\text{ENR} = \frac{\text{noise power difference between hot and cold noise source}}{\text{noise power at } T_0} \tag{13.55}$$

or with the definition of the thermal noise and the noise temperature we write

$$\text{ENR} = \frac{k\left(T_{hot} - T_{cold}\right)B}{kT_0B} = \frac{T_{hot} - T_{cold}}{T_0} \tag{13.56}$$

Here $T_{hot}$ is the equivalent noise temperature of the noise source in the on (hot) state in kelvin, $T_{cold}$ is the equivalent noise temperature for the off (cold) state, and $T_0$ is the reference temperature of 290 K. Most of the time, the reference temperature $T_0$ is the same as the cold noise temperature $T_{cold}$, which reduces Eq. (13.56) to

$$\text{ENR} = \frac{T_{hot}}{T_0} - 1 \tag{13.57}$$

or on a logarithmic scale in decibels as

$$\text{ENR}\big|_{\text{dB}} = 10\log\left(\frac{T_{hot}}{T_0} - 1\right) \tag{13.58}$$

The typical ENR value of noise sources varies between 5 dB and 20 dB. Sources with a high ENR value will generate a higher noise power output, as Eq. (13.58) shows, which makes the noise detection with the ATE easier for low gain devices. However, the disadvantage of high ENR noise sources is that the output impedance is not as stable, which will generate some mismatch error due to a variation in DUT loading. A low ENR source can be built by combining a high ENR source with an attenuator. Noise sources need calibration, like any other RF signal source, to guarantee NIST traceability of the test signals.

### 13.3.2 Noise Measurement Technique with the *Y*-Factor Method

The *Y*-factor method is a popular way of measuring noise figure. Most commercial ATE systems incorporate this approach for measuring noise figure. To use the *Y*-factor method, a noise source with a known *ENR* value is connected to the DUT as shown in Figure 13.20 and the output of the DUT is delivered to a power meter specifically tailored to low noise measurements, commonly referred to as a noise figure meter. Sometimes an RF signal is supplied to the internal mixer of the DUT to down-convert its output before reaching the power meter. The ATE or noise figure meter generates a 28-V DC pulse signal to drive the noise source, which, in turn, generates the noise signal used to drive the DUT. Since the ratio of the two input noise levels is known (i.e., noise source ENR), the noise figure of the DUT can be derived from the noise measurement made at the DUT output. To see this, consider that the noise factor of a DUT is expressed as the ratio of the input SNR to the output SNR according to

$$F = \frac{\text{SNR}_i}{\text{SNR}_0} \tag{13.59}$$

Assuming that the input signal to the DUT is $S_i$ with noise component $kBT_0$ at reference temperature $T_0$ and the gain of the device is $G$ with additive noise component $kBT_e$, then we can express the noise factor above as

$$F = \frac{S_i \big/ kT_0}{GS_i \big/ Gk\left(T_0 + T_e\right)} \tag{13.60}$$

which reduces further to the final result of

$$F = 1 + \frac{T_e}{T_0} \tag{13.61}$$

**Figure 13.20.** Testing the noise figure of a DUT with a noise source.

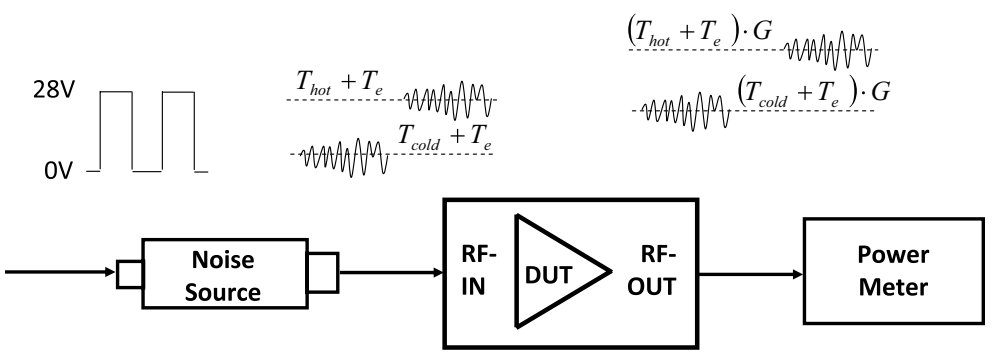

The goal of the *Y*-factor method is to determine the noise factor *F*, which, in turn, is related to the ratio of terms $T_e$ to $T_0$. Since $T_0$ is related to the input source, it is a known quantity. However, $T_e$ is device-dependent and is the missing quantity required to compute the noise factor of a DUT. To obtain this parameter, we make use of the relationship shown in Eq. (13.54), together with the hot and cold noise inputs, to arrive at two measurements of the output noise level as

$$N_{o,hot} = GkB\left(T_{hot} + T_e\right) \tag{13.62}$$

and

$$N_{o,cold} = GkB\left(T_{cold} + T_e\right) \tag{13.63}$$

Recognizing that we have two equations in two unknowns, specifically, *GkB* and $T_e$, we solve using straightforward algebra to arrive at

$$GkB = \frac{N_{o,hot} - N_{o,cold}}{T_{hot} - T_{cold}} \tag{13.64}$$

and

$$T_e = \frac{N_{o,cold}T_{hot} - N_{o,hot}T_{cold}}{N_{o,hot} - N_{o,cold}} \tag{13.65}$$

If we define the *Y*-factor as the ratio of the hot and cold noise power measurements, we write

$$Y = \frac{N_{o,hot}}{N_{o,cold}} \tag{13.66}$$

then Eq. (13.65) can be rewritten as

$$T_e = \frac{T_{hot} - Y \cdot T_{cold}}{Y - 1} \tag{13.67}$$

Replacing this expression back into Eq. (13.61), we write the noise factor as

$$F = 1 + \frac{T_{hot}/T_0 - Y \cdot T_{cold}/T_0}{Y - 1} \tag{13.68}$$

As before, let us select the cold temperature of the noise source as the reference temperature, that is, $T_0 = T_{cold}$; then the noise factor becomes

$$F = 1 + \frac{T_{hot}/T_0 - Y}{Y - 1} \tag{13.69}$$

With the definition of the ENR value given in Eq. (13.57), we can rewrite the noise factor as

$$F = \frac{\text{ENR}}{Y - 1} \tag{13.70}$$

or on a logarithmic dB scale as a noise figure,

$$\text{NF} = 10\log_{10}\left(ENR\right) - 10\log_{10}\left(Y - 1\right) \tag{13.71}$$

For $Y >> 1$, which applies in most practical situations, Eq. (13.71) will simplify to

$$\mathrm{NF} = \left.\mathrm{ENR}\right|_{\mathrm{dB}} - \left.N_{o,hot}\right|_{dBm} + \left.N_{o,cold}\right|_{dBm} \tag{13.72}$$

Both Eqs. (13.71) and (13.72) are commonly used in extracting the noise figure from an ATE with a built-in noise source or a noise source placed on the load board. In some cases, the noise source is replaced with an AWG associated with the ATE, which drives a pseudorandom noise signal with two different power levels. This method has the advantage of having a variable ENR, which can be used to optimize individual test cases with respect of the input power level and dynamic range of the ATE.

### 13.3.3 Noise Measurement Technique with the Cold Noise Method

The cold noise method or gain method is another technique frequently used for measuring the noise figure of a device with a production ATE. This method relies on measuring the cold noise power of a DUT, while terminating the input with a 50-Ω load. This method requires a DUT with a high gain, which often applies to RF-to-base band devices with a high IF gain. Additionally, the method requires a two-step measurement process: First, the gain $G$ of the device is measured, then, as the second step, the noise power $N_{o,cold}$ of the DUT is measured with the input terminated in 50 Ω. Collecting both pieces of information, the noise factor $F$ can be calculated from

$$F = \frac{N_{o,cold}}{kTBG} \tag{13.73}$$

or, in decibels, as

$$\mathrm{NF} = \left.N_{o,cold}\right|_{dBm} - 10\log_{10}(kT) - 10\log_{10}(B) - \left.G\right|_{\mathrm{dB}} \tag{13.74}$$

where $B$ is the bandwidth over which the noise power $N_{o,cold}$ is measured. To simplify its use, we recognize that the thermal noise spectral density $kT$ at 290 K is approximately –174 dBm. Hence, we can rewrite Eq. (13.74) as

$$\mathrm{NF} = \left.N_{o,cold}\right|_{dBm} + 174\ \mathrm{dBm} - 10\log_{10}\left(\frac{T}{290\ \mathrm{K}}\right) - 10\log_{10}(B) - \left.G\right|_{\mathrm{dB}} \tag{13.75}$$

### 13.3.4 Comparison of the Noise Figure Test Methods

The *Y*-factor and the cold noise methods are commonly used to measure the noise figure of a device in production, however, both methods have their advantages and disadvantages.

The *Y*-factor method only measures the ratio of the noise power for two states. Since this is a relative measurement, the absolute accuracy of the test equipment is of less concern. The primary disadvantage of the *Y*-factor method is that the noise source will terminate the DUT with two slightly different input impedances, which can cause some test uncertainty. This disadvantage can be overcome with low ENR noise sources, but this is only applicable to devices with low gain and low noise figure.

The cold noise method has the advantage that it does not require any additional ATE hardware, because it uses no noise source other than a 50-Ω terminating resistor of the turned off RF source. However, this approach is limited to devices with a high gain or a high noise figure, or both. Table 13.1 summarizes the advantages and disadvantages of these two noise figure methods.

Independent of the test method, the noise power associated with a system or device is generally a low power level, which can easily be masked by measurement error. It is important to consider

**Table 13.1.** Comparison of Cold Noise to *Y* Factor Noise Figure Test Method

| Method | Suitable Applications | Advantage | Disadvantage |
|---|---|---|---|
| Cold noise method | High gain or high NF | Accurate at measuring high NF, suitable for a wide frequency range. Easy to implement. | Error can be large when measuring DUT with low gain and low NF. Limited by ATE noise floor. |
| *Y*-factor Method | Wide range of NF | Suitable for DUT with a wide range of NF and frequency regardless of gain. | Error can be large when measuring DUT with high NF. |

## EXAMPLE 13.8

What is the maximum noise figure that can be tested with a noise source with an ENR = 10 dB?

**Solution:**
Using Eq. (13.72) and repeated below, we obtain

$$\mathrm{NF} = \mathrm{ENR}\big|_{\mathrm{dB}} - N_{o,hot}\big|_{dBm} + N_{o,cold}\big|_{dBm}$$

As is evident from the right-hand side of this expression, the NF is maximized when the term on the right-hand side between the brackets is minimized. This occurs when $N_{o,hot} = N_{o,cold}$. As such, the noise figure is equal to ENR, the maximum theoretical limit. However, for a reliable measurement, $N_{o,hot}$ needs to be significantly greater than $N_{o,cold}$.

## EXAMPLE 13.9

What is the maximum power level expected along the measurement path of an ATE when testing the noise figure of a device. The DUT has a NF of 4 dB, the noise source has an ENR = 28 dB and the effective bandwidth of the measurement path is 1 MHz. The cold noise is assumed to be equal to thermal noise at $T$ = 273 K.

**Solution:**
Using Eqs. (13.72), together with the given information, we can write

$$\mathrm{NF} = \mathrm{ENR}\big|_{\mathrm{dB}} - N_{o,hot}\big|_{dBm} + N_{o,cold}\big|_{dBm} \Rightarrow 4 = 28 - N_{o,hot}\big|_{dBm} + N_{o,cold}\big|_{dBm}$$

We are also told that the cold noise is equal to thermal noise at 273 K over a bandwidth of 1 MHz, hence we find that the cold noise power in dBm is equal to

$$N_{o,cold} = 10\log_{10}\left(\frac{kTB}{1\,\mathrm{mW}}\right) = 10\log_{10}\left(\frac{1.38\times10^{-23}\times273\times1\times10^{6}}{1\times10^{-3}}\right) = -114.2\ \mathrm{dBm}$$

Substituting this cold noise power into the expression written above, we solve

$$N_{o,hot} = 28 - 4 - 114.2 = -90.2\ \mathrm{dBm}$$

Accountingfor the random noise crest factor corresponding to 11 dB, we estimate the peak power to be about –90.2 dBm +11 dB or –79.2 dBm.

**Exercises**

| | | |
|---|---|---|
| **13.12.** | What is the NF of a DUT if the noise source has an ENR of 32 dB, and the hot and cold noise power is –90.2 and –120.3 dBm, respectively? | ANS. 1.9 dB. |
| **13.13.** | What is the noise factor *F* of a DUT if the noise source has an ENR of 32 dB and the *Y*-factor is 900? | ANS. 1.76. |
| **13.14.** | What is the peak power level expected at the output of a DUT if it has an NF of 3 dB, the noise source has an ENR = 31 dB, and the effective bandwidth of the measurement path is 10 MHz. The cold noise is assumed to be equal to thermal noise at $T$ = 225 K. | ANS. –66.1 dBm. |

that the noise figure of the ATE will be tested with an ATE with its own noise floor, which needs to be calibrated out. In the cold noise method the device input is terminated and the thermal noise is measured. At the output, a power measurement is performed with a calibrated power meter. For *Y*-factor it's a relative measurement and the measurement path needs to be treated as second stage in the deFriis equation. The other caveat is that noise signals will have a high crest factor, which makes the measurement on top of the low level unrepeatable when selecting a short integration time. Averaging the noise power is good practice in order to have a stable reading with a good repeatability.

## 13.4 PHASE NOISE

Phase noise is a critical performance parameter of RF systems and devices. It is related to the power spectral density of noise around a carrier and is typically expressed in $rad^2/Hz$ or on a logarithmic scale as dBc/Hz. Here dBc refers to the ratio of power of a signal or noise relative to the power in a carrier expressed in decibels. The theoretical background of phase noise was described previously in Section 12.3.2. Here we will discuss methods for measuring the phase noise of an RF device and discuss their limitations.

A frequency synthesizer constructed from a reference oscillator and PLL is part of all RF systems and is included in most RF devices. The reference oscillator is in most test applications bypassed with a reference signal from the ATE to synchronize the timing system of the DUT with the ATE. The PLL is used to translate a reference frequency to an RF frequency so that a specific signal-processing task, like mixing, can be performed. Understanding the functionality of the PLL is beneficial for understanding phase noise test techniques.

Figure 13.21 illustrates a basic block diagram of a frequency synthesizer. Here a reference signal is applied to the input of PLL whose output generates an RF signal. The PLL consists of a two-input phase/frequency detector (PFD), followed by a charge pump, loop filter, and voltage-controlled oscillator (VCO). The loop filter acts to smooth out any quick changes appearing in the phase of the input reference signal, thereby maintaining a steady control signal at the input of the VCO. The output of the VCO is then feedback via a divider circuit to the second input of the phase detector. Collectively, the components of the PLL form a negative feedback loop, whereby the phase and frequency of the divider output is adjusted such that the phase difference between the reference and the feedback signal is a constant. This results in the frequency of the feedback

**Figure 13.21.** Principle block diagram of a PLL with phases/frequency detector (PFD), charge pump, loop filter, VCO and frequency divider.

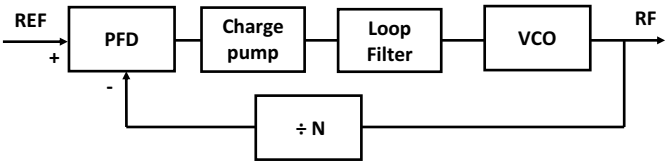


signal to be exactly equal to the reference frequency. As a result, the output of the VCO (denoted $f_{RF}$) will be $N_{PLL}$ times the input reference frequency (denoted $f_{Ref}$), that is,

$$f_{RF} = N_{PLL} \times f_{REF} \tag{13.76}$$

where $N_{PLL}$ is the divider ratio of the divider block.

Not only will the reference frequency $f_{REF}$ be transformed to the RF signal of the VCO, but so too will the phase noise of the reference signal. For the situation where the reference signal is the sole phase noise contributor, the phase noise of the RF signal can be assumed to be

$$£_{RF}(f)\big|_{\text{dBc/Hz}} = £_{REF}(f)\big|_{\text{dBc/Hz}} + 20\log_{10}(N_{PLL}) \tag{13.77}$$

The dynamics of the PLL is a function of all elements of the PLL but is generally dominated by the dynamics of the loop filter. Since the loop filter is designed for a small bandwidth operation, the PLL has a relatively slow settling and lock time. The phase noise characteristics of the PLL are dependent on the characteristics of the loop filter and also on the noise characteristics associated with the reference input and the VCO. It should be noted that any frequency error associated with the reference signal translates directly to the PLL output, however, the PLL itself will not introduce any frequency errors because its input–output behavior is governed by Eq. (13.76).

For frequencies within the loop filter bandwidth, the phase PSD of the PLL is dominated by the noise of the reference signal. However, for frequencies outside the loop filter bandwidth, the PLL output PSD is dominated by the noise of the VCO. For this reason, the spurious free dynamic range is often part of the required set of tests performed on a synthesizer. Common sources for these spurs are the reference signal with its harmonics and the divider.

### 13.4.1 Measuring Phase Noise Using Spectral Analysis

One of the most common ways of measuring the phase noise of a device with an ATE is through an FFT analysis of a time-sampled signal. As such, the phase noise is defined in terms of the spectrum of a signal captured by a digitizer. Specifically, phase noise is defined as the ratio of the power in a 1-Hz bandwidth offset from the carrier frequency $f_c$ by a frequency $f$ denoted by $P_{SSB}$ to the power in the tone at $f_c$, denoted by $P_S$, that is,

$$£(f)\big|_{\text{dBc/Hz}} = 10\log_{10}\left(\frac{P_{SSB}}{P_S}\right) \tag{13.78}$$

A diagram illustrating the components of this measurement is shown in Figure 13.22. Often, the offset power component $P_{SSB}$ is measured with a bandwidth other than 1 Hz. This is particularly true when working with an FFT analysis where the resolution bandwidth of an $N$-point FFT is $F_s/N$. As such, Eq. (13.78) is modified to account for this bandwidth difference, resulting in the phase noise being described as

## EXAMPLE 13.10

The phase noise of the output of a PLL at an offset of 100 kHz from the carrier is equal to –100 dBc/Hz. Write a mathematical description of the phase noise as a function of frequency, and plot the result from 1 to 200 kHz on a log-linear scale.

**Solution:**
Assuming that thermal noise is solely responsible for the phase noise from a PLL, a Lorentzian process can be used to describe the PSD. Using Eq. (13.72), we write

$$\mathcal{L}_{RF}(f) = \frac{1}{2} S_{\phi,RF}(f) = \frac{a_{PLL}}{\pi^2 a_{PLL}^2 + f^2} \text{ rad}^2/\text{Hz}$$

Using the given information, $\mathcal{L}_{RF}(100 \text{ kHz})\big|_{\text{dBc/Hz}} = -100$ dBc/Hz, we solve for the phase noise in rad²/Hz and find

$$\mathcal{L}_{RF}(100 \text{ kHz}) = 10^{\left(\mathcal{L}_{PLL}|_{\text{dBc/Hz}}\right)/10} = 10^{-10} \text{ rad}^2/\text{Hz}$$

Substituting this result into the expression listed above, with $f = 100 \times 10^3$ Hz, we write

$$10^{-10} = \frac{a_{PLL}}{\pi^2 a_{PLL}^2 + \left(100 \times 10^3\right)^2}$$

This leads to the coefficient $a_{PPL} = 1$ or $10^9$, because either result will model the phase noise correctly. Selecting the former value, we find the following mathematical formula for the phase noise as

$$\mathcal{L}_{RF}(f) = \frac{1}{\pi^2 + f^2} \text{ rad}^2/\text{Hz}$$

Expressing the above in dBc/Hz, we can write

$$\mathcal{L}_{RF}(f)\big|_{\text{dBc/Hz}} = 10\log_{10}\left(\mathcal{L}_{RF}(f)\right) = 10\log_{10}\left(\frac{1}{\pi^2 + f^2}\right)$$

Approximating the phase noise as two straight lines, we can write

$$\mathcal{L}_{RF}(f)\big|_{\text{dBc/Hz}} \approx \begin{cases} -20\log_{10}(\pi), & f < \pi \\ -20\log_{10}(f), & f > \pi \end{cases}$$

A plot of the phase noise in dBc/Hz over a 200 kHz frequency interval is shown below:

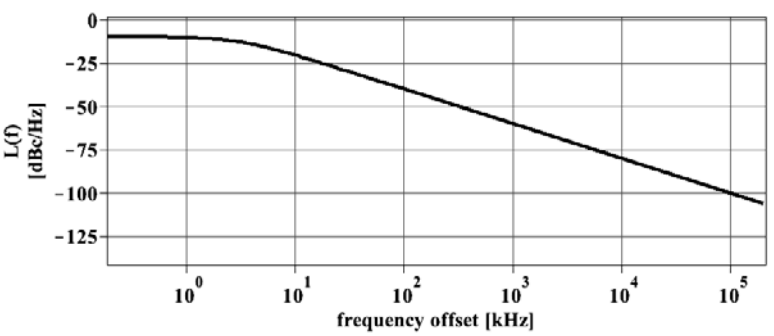

## EXAMPLE 13.11

The phase noise of a VCO needs to be tested. A 20-MHz reference signal is sourced from an ATE to a PLL with a feedback divider ratio of 100. If the ATE reference has a phase noise of –120 dBc/Hz, what effect does this noise have on the PLL output?

**Solution:**
To measure the phase noise of the VCO, we need to make sure that the impact of the phase noise of the reference source is significantly lower than that of the VCO. One typically assumes that the source phase noise is about 10 dB less than the contribution from the VCO. Using Eq. (13.77), we compute the PLL RF output phase noise due to the reference as

$$£_{RF}(f)\big|_{\text{dBc/Hz}} = £_{\text{REF}}(f)\big|_{\text{dBc/Hz}} + 20\log_{10}(N_{PLL}) = -120\ \text{dBc/Hz} + 20\log_{10}\left(\frac{2\ \text{GHz}}{20\ \text{MHz}}\right) = -80\ \text{dBc/Hz}$$

Clearly, the effect of the reference source phase noise is increased by 40 dBc/Hz on account of the multiplicative frequency effect of the PLL.

$$£(f)\big|_{\text{dBc/Hz}} = 10\log_{10}\left(\frac{P_{SSB}}{P_S}\right) - 10\log_{10}\left(\frac{F_s}{N}\right) \tag{13.79}$$

or as

$$£(f)\big|_{\text{dBc/Hz}} = P_{SSB}\big|_{\text{dBm}} - P_S\big|_{\text{dBm}} - 10\log_{10}\left(\frac{F_s}{N}\right) \tag{13.80}$$

In terms of the FFT analysis, here $P_s|_{dBm}$ represents the magnitude of the power in dBm in the FFT bin corresponding to the carrier and $P_{ss}|_{dBm}$ represents the magnitude of the power in the FFT bin at some integer multiple of $F_s/N$ offset from the carrier. In terms of the spectral coefficients

**Figure 13.22.** Illustrating the components of a phase noise metric from a spectrum analysis of a signal.

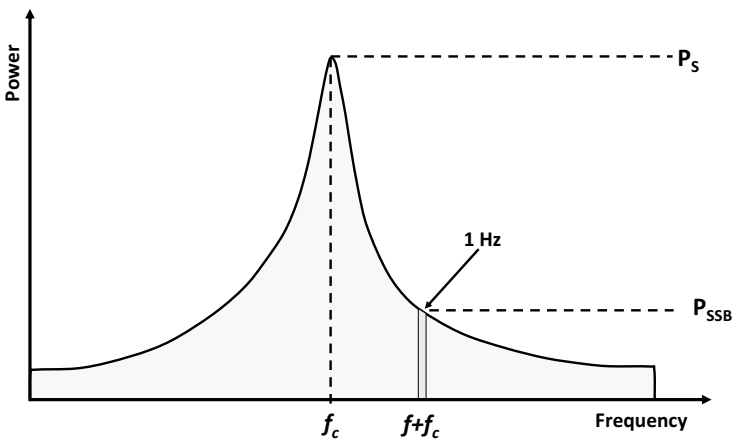

derived from an $N$-point FFT analysis of the captured data set [recall Eq. (13.1)], these two power terms would be computed according to

$$P_S\big|_{\text{dBm}} = 10\log_{10}\left(\frac{c_{M_S,RMS}^2/Z_0}{1\text{ mW}}\right) \tag{13.81}$$

and

$$P_{SSB}\big|_{\text{dBm}} = 10\log_{10}\left(\frac{c_{M_{SSB},RMS}^2/Z_0}{1\text{ mW}}\right) \tag{13.82}$$

where it is assumed that the carrier signal is located in bin $M_S$, the offset spectral component of interest is located in bin $M_{SSB}$, and the ADC is assumed to be terminated in real-valued impedance $Z_0$.

For this measurement it is critical to have the carrier signal coherent with the digitizer-sampling frequency $F_s$; otherwise, power will leak across different spectral bins. This will require synchronizing the DUT with the timing system of the ATE by applying a reference signal to the PLL. Since the phase noise of the reference signal can have an impact on the measured phase noise, it is necessary that the reference signal have a better phase noise than the PLL itself. This low phase noise can be achieved directly by using an ATE reference source with a very low phase noise component, or indirectly, by using a higher-frequency source whose output is divided down in frequency, which, in turn, reduces its effective phase noise.

For a reference signal with frequency $f_{RF}$ and phase noise $£(f_{Reference})$ applied to the input of a PLL with output frequency $f_{RF}$, the phase noise seen by the DUT can be described by

$$£(f_{RF}) = £(f_{reference}) + 20\log_{10}\left(\frac{f_{RF}}{f_{reference}}\right) \tag{13.83}$$

Here we see that the latter term can magnify the effect of the phase noise of the reference signal. As such, the phase noise of the reference source is a critical parameter of the ATE.

Another important consideration when testing the phase noise of a device is the measurement dynamic range of the ATE. ATE instruments must be capable of measuring both the power of the carrier $P_S$ and the power at some offset from the carrier, $P_{SSB}$. Since these two powers may differ in magnitude by several orders of magnitude, a critical review on the ATE noise floor and measurement path compression point is necessary before undertaking this measurement.

Sometimes a performance metric related to the integration of the phase noise over the channel bandwidth is desired. This is called the integrated phase noise and is expressed in various formats. For a channel defined between frequencies $f_l$ and $f_u$, we can define the integrated phase noise expressed in squared radians as

$$\Phi_{PN} = 2\times\int_{f_l}^{f_u} £(f)\,df \tag{13.84}$$

In terms of the FFT data, the integrated phase noise expressed in square radians would be computed according to

$$\Phi_{PN} = \frac{F_s}{N}\times\frac{\sum_{k=M_l}^{M_u} c_{k,RMS}^2}{c_{M_S,RMS}^2} \tag{13.85}$$

where $M_l$ and $M_u$ represents the lower and upper FFT bins corresponding to the frequency edges of the channel. Often we speak in terms of the RMS phase error. This is simply the square root of the integrated phase noise,

$$\sigma_{\phi}\big|_{\text{rad}} = \sqrt{\Phi_{PN}} \tag{13.86}$$

To convert this quantity to degrees, we follow

$$\sigma_{\phi}\big|_{\text{degrees}} = \frac{180}{\pi}\sqrt{\Phi_{PN}} \tag{13.87}$$

Sometimes one is interested in the RMS frequency error or residual FM. The residual FM is expressed in Hz and is defined as

$$\sigma_{FM}\big|_{\text{Hz}} = \sqrt{2\times\int_{f_l}^{f_u} \pounds(f)\cdot f^2\, df} \tag{13.88}$$

The integrated phase noise test is easy to implement in production, however, it has some limitations. The first is inherent in the definition itself. The measured power is the combined power of phase noise and amplitude noise. For many cases, the phase noise contribution is dominant so that we can assume that the amplitude noise portion is negligible. The other limitation is a result of the performance limitations of the ATE. The inherent phase noise of the ATE LO synthesizer and reference source can limit the minimum measurable phase noise. Furthermore, this method requires a large measurement dynamic range, as the carrier is always present during this measurement. Few commercial ATE can block specific frequencies in the captured bandwidth. Hence, the carrier will establish the highest power level in the measurement path of the ATE.

## EXAMPLE 13.12

A frequency synthesizer produces an output frequency at 1.20117 GHz. What is the phase noise of this synthesizer at a frequency offset of 4.8828 MHz if the output is digitized at a sampling rate of 5 GHz using an ADC with an input impedance of 50 Ω. Subsequently, a 2048-point FFT analysis reveals the following information:

$$\left|\text{FFT}\{x[n]\}\right| = \begin{cases} 1.11\times10^{-6} & \text{Bin} = 0 \\ \vdots & \\ 1.21 & \text{Bin} = 492 \\ \vdots & \\ 6.23\times10^{-3} & \text{Bin} = 494 \\ \vdots & \end{cases}$$

**Solution:**

According to the given information, the expect bin for the carrier is in FFT bin

$$M_c = \frac{f_c}{F_s}N = \frac{1.2012\ \text{GHz}}{5\ \text{GHz}}\times 2048 = 492$$

Likewise, the offset bin relative to the carrier is found from the following:

$$M_{c+offset} = \left(\frac{f_c + f_{offset}}{F_s}\right)N = \left(\frac{1.2012\ \text{GHz} + 4.9928\ \text{MHz}}{5\ \text{GHz}}\right)\times 2048 = 494$$

According to the given FFT data, we can compute the spectral coefficients using Eq. (13.1), to arrive at

$$c_{492,rms} = \frac{\sqrt{2}}{2048} \times 1.21 = 835.55 \times 10^{-6}$$

$$c_{494,rms} = \frac{\sqrt{2}}{2048} \times 1 \times 10^{-5} = 4.30 \times 10^{-6}$$

Finally, the power associated with each term is found, by application of Eqs. (13.81), and (13.82) to be

$$P_S\big|_{\text{dBm}} = 10\log_{10}\left(\frac{c_{492,RMS}^2 / 50\ \Omega}{1\ \text{mW}}\right) = -48.55\ \text{dBm}$$

$$P_{SSB}\big|_{\text{dBm}} = 10\log_{10}\left(\frac{c_{494,RMS}^2 / 50\ \Omega}{1\ \text{mW}}\right) = -94.31\ \text{dBm}$$

Finally, the phase noise at a frequency offset of 4.9928 MHz is found, using Eq. (13.80), to be

$$\pounds(4.9928\ \text{MHz})\big|_{\text{dBc/Hz}} = P_{SSB}\big|_{\text{dBm}} - P_S\big|_{\text{dBm}} - 10\log_{10}\left(\frac{F_s}{N}\right) = -94.31\ \text{dBm} - (-48.55\ \text{dBm}) - 10\log_{10}\left(\frac{5\times 10^9}{2048}\right),$$

reducing to

$$\pounds(4.9928\ \text{MHz})\big|_{\text{dBc/Hz}} = -109.64\ \text{dBc/Hz}$$

## 13.4.2 PLL-Based Phase Noise Test Method

The spectral analysis approach to phase noise extraction is prone to AM modulation interference. Two techniques that avoid this problem are the PLL-based and delay line phase noise test methods. A drawback to these methods, though, is that they require load board circuits to complete the test setup.

The basic concept of the PLL-based phase noise test method is to mix the output of a DUT using a quadrature mixer acting as a phase discriminator as depicted in Figure 13.23. This requires a low phase noise reference source, which is phase locked to the DUT. The PLL will force the feedback signal to be at 90° out of phase with respect to the DUT signal. This biases the phase detector in its linear region at the most sensitive point. In this method, the short-term phase fluctuations of the DUT are translated directly to low-frequency voltage fluctuations, which can then be measured by a low-frequency analyzer. We assume that the signal from the DUT can be described as $v_{DUT}(t) = \sin[2\pi f_c t + \phi_{DUT}(t)]$, where $\phi_{DUT}(t)$ is the phase signal of interest. Also, due to the feedback action associated with the PLL, the signal being fed back to the other input of the phase detector is $v_{Ref}(t) = \sin = (2\pi f_c t - \pi/2) - \cos(2\pi f_c t$. Then at the output of the phase detector we would see

$$v_{PD}(t) = -k_{PD}\sin\left[2\pi f_c t + \phi_{DUT}(t)\right]\cos\left(2\pi f_c t\right) \approx -\frac{k_{PD}}{2}\left[\sin\left[2\cdot 2\pi f_c t + \phi_{DUT}(t)\right] + \sin\left[\phi_{DUT}(t)\right]\right] \quad \textbf{(13.89)}$$

Passing the mixer signal through a low-pass filter removes the double frequency term, resulting in the filter output signal as

$$v_{LPF}(t) = -\frac{k_{PD}}{2}\sin\left[\phi_{DUT}(t)\right] \quad \textbf{(13.90)}$$

**Figure 13.23.** Phase detector (PD) method to measure phase noise.

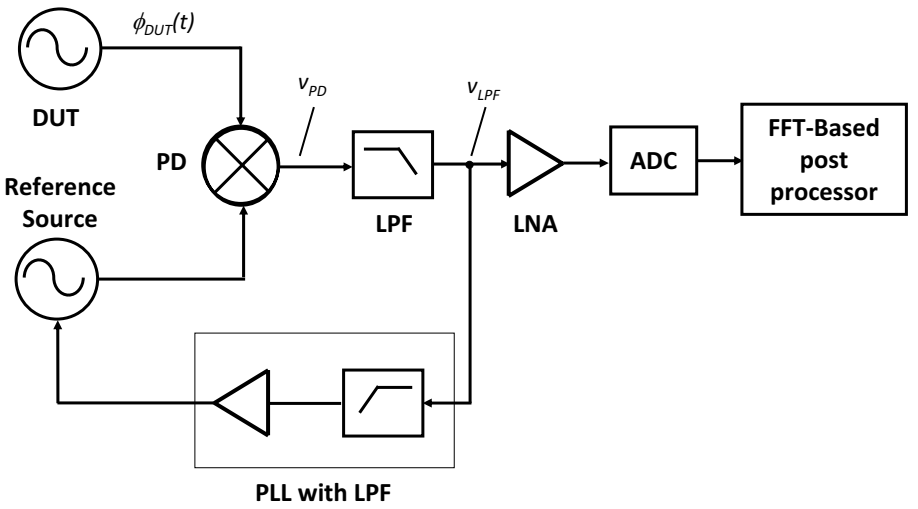


Assuming that the phase variation is small, the filtered output of the phase detector can be approximated by

$$v_{LPF}(t) \approx -\frac{k_{PD}}{2} \cdot \phi_{DUT}(t) \tag{13.91}$$

Taking the Laplace transform of the above expression leads to

$$V_{LPF}(s) \approx -\frac{k_{PD}}{2} \cdot \Phi_{DUT}(s) \tag{13.92}$$

where $\Phi_{DUT}(s)$ is the Laplace transform of $\phi_{DUT}(t)$ and $V_{LPF}(s)$ is the Laplace transform of $v_{LPF}(t)$. The magnitude of the transfer function from the output of the DUT to the output of the low-pass filter can then be written as

$$\left|H(jf)\right| = \frac{\left|V_{LPF}(jf)\right|}{\left|\Phi_{DUT}(jf)\right|} = \frac{k_{PD}}{2} \tag{13.93}$$

Consequently, the spectrum of the voltage signal that appears at the output of the LPF can be written in terms of the phase spectrum of the DUT as

$$S_{v,LPF}(f) = \left|H(jf)\right|^2 S_{\phi,DUT}(f) \tag{13.94}$$

which can just as easily be written in terms of the phase noise of the DUT as

$$£_{DUT}(f) = \frac{4}{k_{PD}^2} £_{v,LPF}(f) \tag{13.95}$$

Except for the scale factor pertaining to the phase detector, the measurement of the phase noise using the PLL-based approach is carried out in the exact same way using the FFT spectral analysis approach of the previous method. Since the phase noise is dependent on the phase detector gain

$k_{PD}$, this quantity must be accurately determined through a calibration procedure during the load board setup time.

For large phase noise signals, especially at close-in offset frequencies, the linear assumption pertaining to Eq. (13.91) will be wrong. Moreover, for offset frequencies within the loop bandwidth of the PLL, the PLL tracks the phase signal of the DUT and cancel it. This will limit this PLL-based method to frequencies greater than the loop bandwidth. The advantage of this method is that the carrier itself is canceled due to the quadrature condition of the mixer, which improves the dynamic range of the signal processing, including the LNA and ADC. The other advantage as noted before is that this method separates the AM component from the phase noise component, which allows testing of the true phase noise. The PLL-based phase noise test technique is by far the most accurate method, but also the most expensive in terms of equipment and implementation cost.

### 13.4.3 Delay-Line Phase Noise Test Method

The other approach that measures the true phase of the DUT is the delay-line phase noise test method.[6] Figure 13.24 shows the delay line/mixer implementation of a phase discriminator to measure the phase noise of a DUT. The DUT signal is split into two channels: One channel is applied directly via a phase shifter to the double balanced mixer, the other channel is delayed through a time delay element and then applied to the mixer. The tunable phase shifter provides a means to adjust the output signal for maximum sensitivity. In the time domain, the output of the phase detector/LFP can be shown[6] to be equal to

$$v_{LPF}(t) = k_{PD}\left[\phi_{DUT}(t) - \phi_{DUT}(t-\tau_d)\right] \tag{13.96}$$

where $\phi_{DUT}(t)$ the instantaneous phase signal associated with the DUT and $\tau_d$ is the propagation delay of the delay line minus the delay introduced by the phase shifter. In essence, this circuit converts phase fluctuations into voltage fluctuations, thereby removing the carrier from the measurement path. The noise floor of this system is typically not critical since the carrier does not limit the dynamic range of this method and an LNA with a decent noise figure can significantly improve the measurement sensitivity. Furthermore, the output signal from the LNA is digitized and an FFT is used to extract the phase noise of the DUT. To quantify this, consider taking the Laplace transform of Eq. (13.96) according to

$$V_{LPF}(s) = k_{PD}\left(1 - e^{-s\tau_d}\right)\Phi_{DUT}(s) \tag{13.97}$$

where $\Phi_{DUT}(s)$ is the Laplace transform of $\phi_{DUT}(t)$. The magnitude of the transfer function from the output of the DUT to the output of the low-pass filter can then be written as

$$\left|H(jf)\right| = \frac{\left|V_{LPF}(jf)\right|}{\left|\Phi_{DUT}(jf)\right|} = k_{PD}\left|1 - e^{-j2\pi f\tau_d}\right| = 2k_{PD}\sin(\pi f\tau_d) \tag{13.98}$$

Consequently, the spectrum of the voltage signal that appears at the output of the LPF can be written in terms of the phase spectrum of the DUT as

$$S_{v,LPF}(f) = \left|H(jf)\right|^2 S_{\phi,DUT}(f) \tag{13.99}$$

which can just as easily be written in terms of the phase noise of the DUT as

$$\pounds_{DUT}(f) = \frac{1}{4k_{PD}^2\sin^2(\pi f\tau_d)}\pounds_{v,LPF}(f) \tag{13.100}$$

**Figure 13.24.** Delay line method to measure phase noise.

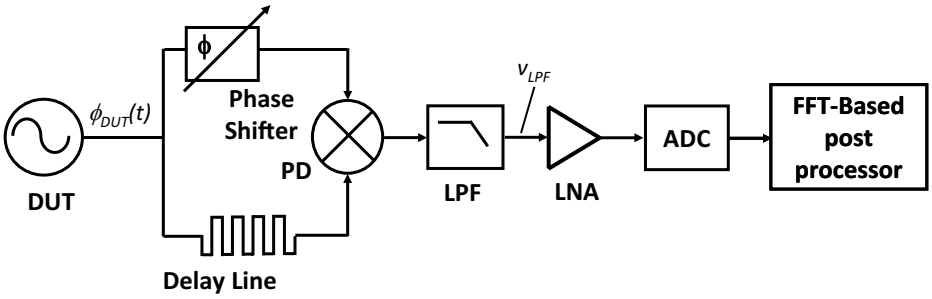


**Table 13.2.** Comparison of different methods for measuring phase noise.

| Phase Noise Test Method | Advantage | Disadvantage |
|---|---|---|
| **Spectrum analysis method** | • Easy setup with RF ATE<br>• No calibration required<br>• No external circuits required on load board | • AM and phase noise can not be separated<br>• No carrier suppression require high dynamic range<br>• Measurement accuracy limited by ATE LO and reference source phase noise |
| **Phase detector Method** | • AM and phase noise separated<br>• Carrier suppression allow high dynamic range | • Test method require external circuits on load board<br>• calibration required<br>• complicated setup with calibration |
| **Delay line method** | • Suitable for drifting oscillators<br>• No reference oscillator required<br>• AM suppression<br>• Carrier suppression allow high dynamic range | • Complicated setup requiring external components on load board<br>• Complicated calibration procedure<br>• Restricted measurement range |

Once again, we see that the phase noise of the DUT is simply obtained through an FFT analysis of the signal captured by the ADC with the appropriate calibration factors incorporated—for example, phase detector gain, delay, LNA and ADC measurement path gain, and so on.

### *Comparison of the Phase Noise Test Methods*

Table 13.2 compares the three phase noise test methods described earlier. It is obvious that the spectrum analysis method is the easiest to set up with an ATE, because no external circuits are required. However, it has the disadvantage that the carrier is not suppressed, which limits the dynamic range of the measurement. Furthermore, this method does not separate AM signal effects from the phase noise. Some ATEs have a built-in phase noise module with a delay line, which significantly improves the measurement dynamic range. The carrier will be suppressed and the method produces a signal proportional to the phase noise without any AM effects. It also does not require an expensive low phase noise reference source.

## 13.5 VECTOR SIGNAL ANALYSIS

Vector signal analysis (VSA) is the measurement of complex dynamic signals, which might be time-varying or complex-modulated. Time-varying signals, like burst, gated, pulsed, or transient

## Exercises

**13.15.** The phase noise of an oscillator at an offset of 500 kHz from the carrier is equal to –90 dBc/Hz. Assuming that the noise process is best described as Lorentzian, write a general description of the phase noise as a function of frequency.

ANS. $\mathcal{L}_{OSC}(f)\big|_{\text{dBc/Hz}} = 10\log_{10}\left(\frac{250}{250^2\pi^2 + f^2}\right)$

**13.16.** The phase noise of a VCO needs to be tested. A 320-MHz reference signal is sourced from an ATE to a PLL with a feedback divider ratio of 16. If the ATE reference has a phase noise of –105 dBc/Hz, what is the minimum level of VCO phase noise that can be measured with this setup?

ANS. –70.92 dBc/Hz; assuming 10 dB margin.

**13.17.** The phase noise of a VCO within a PLL with a feedback divider ratio of 32 is to be tested using a delay-line phase noise test setup. The VCO is to be tuned to a frequency within the ISM frequency band at 2.450 GHz, and the phase noise is to be measured at approximately 1 MHz offset. What frequency should be sourced to the PLL from the ATE, and what sampling frequency should the digitizer use to collect 4096 samples? What is the exact offset frequency from the VCO output?

ANS. $F_s = 5$ GHz; $F_{REF,ATE} = 76.5625$ MHz; $f_{offset} = 1.2207$ MHz.

**13.18.** The phase noise of an oscillator is to be tested using a PLL-based phase noise test setup. The oscillator is tuned to a frequency of 1.401367 GHz. What is the phase noise of this device at a frequency offset of 4.8828 MHz if the output is digitized at a sampling rate of 5 GHz using an ADC with an input impedance of 50 Ω. Subsequently, a 2048-point FFT analysis reveals the following information:

$$FFT\{x[n]\} = \begin{cases} 3.42\times10^{-6} & \text{Bin} = 0 \\ \vdots & \\ 1.51 & \text{Bin} = 287 \\ 8.23\times10^{-3} & \text{Bin} = 288 \\ 6.23\times10^{-3} & \text{Bin} = 289 \\ \vdots & \end{cases}$$

ANS. –112.16 dBc/Hz

signals, change their properties during the measurement sweep. Complex modulated signals cannot solely be described in terms of a simple analog modulation (see Chapter 12, Section 12.5), but instead require more elaborate descriptions such as quadrature amplitude modulation (QAM). When measuring the power with a power meter or spectrum analyzer, it is necessary that the power will be stable during the measurement time. A traditional spectrum analyzer sweeps a narrow-band filter across a frequency range, sequentially measuring one frequency at a time. This requires a repetitive or constant signal. Furthermore, this technique provides only a scalar measurement, such as the magnitude of a signal. In contrast to this, a vector analysis measures both the magnitude and phase of a signal as a function of time. By applying an FFT function, this result can be transformed into the frequency domain. Figure 13.25 shows the block diagram of a typical vector signal analyzer.[1,2]

When comparing the block diagram in Figure 13.25 with a typical ATE architecture (see Chapter 2), it appears that the hardware implementation of a vector signal analyzer is similar to the ATE architecture. The DSP function can be built as firmware in the operating system or as part of the test program. This makes an ATE a good solution for vector analysis of complex RF signals. The only critical task will be the implementation of the required analysis software. In the following subsection, we will discuss the most common techniques used for vector analysis of RF signals.

### 13.5.1 In-Phase and Quadrature Signal Representation

RF circuits process information that is carried by complex-valued signals. Since a complex signal at any instant of time has two independent signal components, we can refer to such signals as phasors or, equivalently, as two-dimensional vectors. To gain an understanding of RF signals, let us define the concept of an analytic signal.

If the negative frequency components of a signal are discarded, such as through the process of quadrature modulation, then the modulated signal will take on complex values as a function of time. This is in contrast to the signal prior to modulation where it varies as a function of time as real-valued quantities. It is customary to describe base-band signals with real-value functions of time [e.g., $A\sin(2\pi f \cdot t)$], and bandpass signals with complex or analytic signals [e.g., $A\sin(2\pi f \cdot t) + jA\cos(2\pi f \cdot t)$]. In general, for any signal $x(t)$ the corresponding analytic representation is given by $x(t) + j \cdot \hat{x}(t)$, where $\hat{x}(t)$ is known as the Hilbert transform of the real-valued signal $x(t)$. The Hilbert transform is simply an operation that phase shifts $x(t)$ by 90 degrees over all positive frequencies. It is important for the reader to recognize that the actual $j$ operator is not transmitted with the signal. Rather, it is implicit in the modulation scheme whereby the signals are made orthogonal to one another. As such, the signals can easily be separated from one another at the receiver end.

From the theory of complex numbers, a complex quantity can be represented by a rectangular formulation, such as $x(t) + j \cdot \hat{x}(t)$ or, equivalently in magnitude and phase form, as $\sqrt{x^2(t) + \hat{x}^2(t)} \cdot e^{j\phi(t)}$. At any instant in time, the signal will be complex in value. This complex number can be plotted in the complex plane using rectangular coordinates as shown in Figure 13.26. Here the horizontal axis is denoted as $I$ and is equal to the real part of the signal, $x(t)$. Similarly, the vertical axis is denoted as $Q$ and is equal to the imaginary part of the signal $\hat{x}(t)$. It is tradition to refer to $I$ and $Q$ as the in-phase and quadrature signals, respectively. In this textbook, we shall refer to the complex or analytic signal as the $IQ$ signal.

### 13.5.2 Test of Relative Phase

Figure 13.27 shows a typical RF-to-base-band transceiver device, which might also be part of an RF-to-digital system-on-chip (SOC). For more complex digital modulation schemes, the phase of the signal (albeit a modulated signal) is important for obtaining measures of system performance.

**Figure 13.25.** Block diagram of a typical vector signal analyzer.

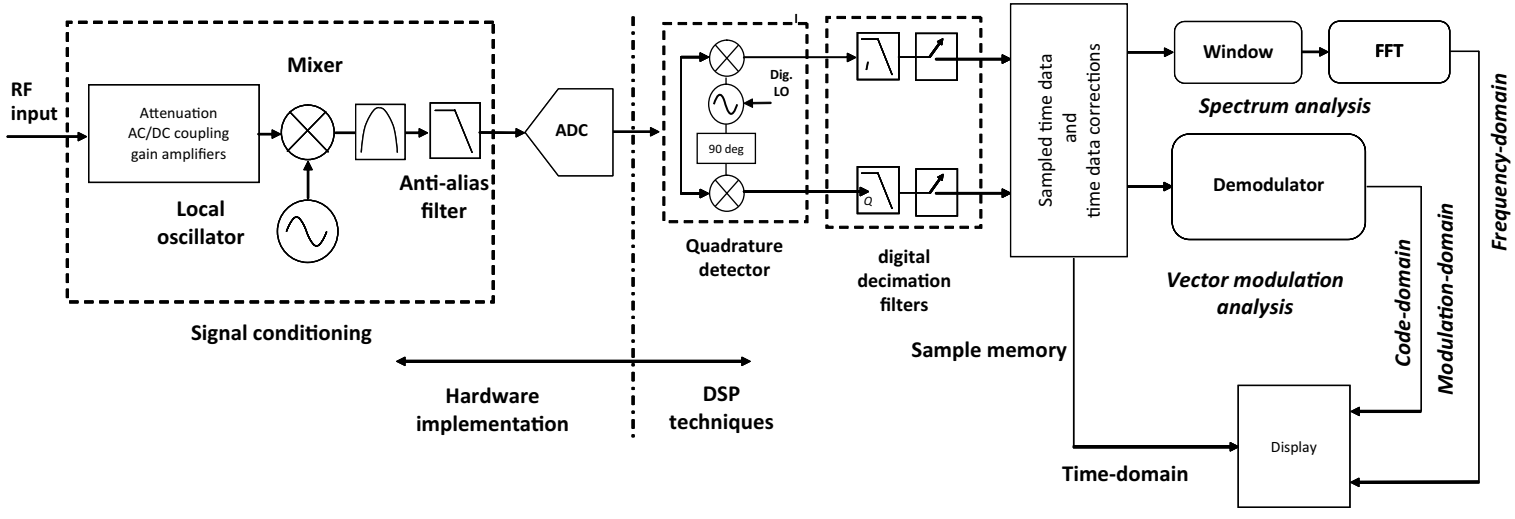

**Figure 13.26.** Arbitrary signal in the complex IQ-plane.

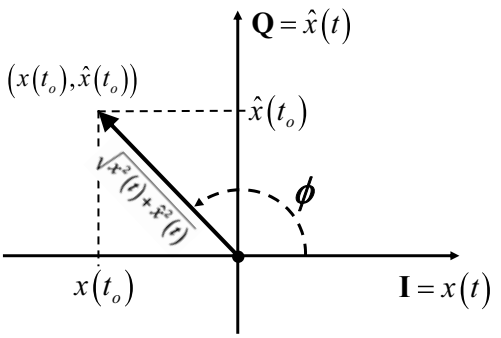


**Figure 13.27.** Typical RF transceiver DUT.

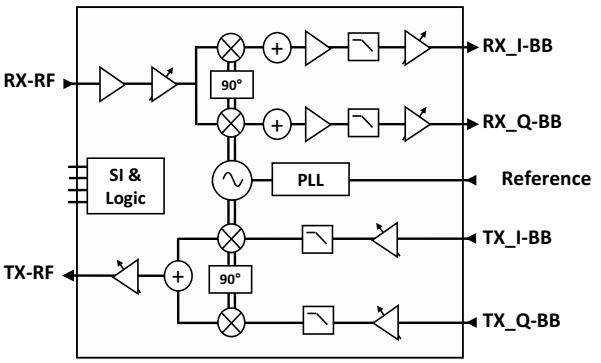


## EXAMPLE 13.13

An ideal 1-GHz continuous wave sinusoidal signal is passed through a quadrature modulator, resulting in an *IQ* signal having the following form: $\sin(2\pi 10^9 \cdot t) + j \cdot \cos(2\pi 10^9 \cdot t)$. Plot the *I* and *Q* components of this complex signal. Also, plot the magnitude and instantaneous phase of this signal.

**Solution:**
The *I* and *Q* signals can be described as

$$I(t) = \sin\left(2\pi 10^9 \cdot t\right)$$
$$Q(t) = \cos\left(2\pi 10^9 \cdot t\right)$$

A plot of these two signals superimposed on the same time scale is shown below:

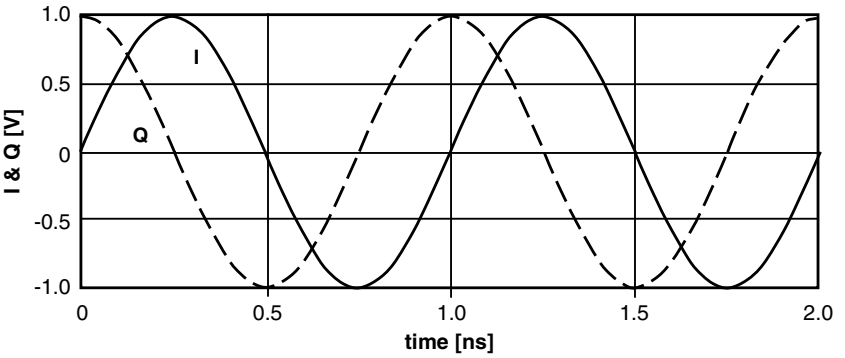


Expressing the complex signal in magnitude and phase form, we write

$$M(t)\cdot e^{j\phi(t)} = \sin\left(2\pi 10^9\cdot t\right) + j\cdot\cos\left(2\pi 10^9\cdot t\right)$$

where

$$M(t) = \sqrt{\sin^2\left(2\pi 10^9\cdot t\right) + \cos^2\left(2\pi 10^9\cdot t\right)} = 1$$

$$\phi(t) = \tan^{-1}\left[\frac{\cos\left(2\pi 10^9\cdot t\right)}{\sin\left(2\pi 10^9\cdot t\right)}\right] = 2\pi 10^9\cdot t$$

A plot of these two components for the RF complex signal is shown below:

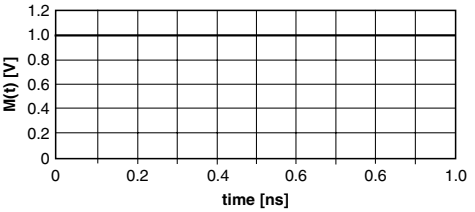


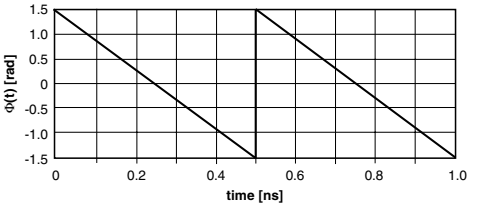


In terms of a vector in the complex *IQ* plane, we see from the results above that the vector associated with the ideal reference source has a constant magnitude of unity and rotates uniformly around thecomplex plane in a counterclockwise motion with frequency $2\pi 10^9$ radians per second.

## EXAMPLE 13.14

A 1-GHz continuous wave sinusoidal signal is pass through a quadrature modulator resulting in an *IQ* signal having the following form: $\sin\{2\pi 10^9\cdot t - \pi/5\} + j\cdot\cos\{2\pi 10^9\cdot t + \pi/8\}$. Plot the *I* and *Q* components of this complex signal and the corresponding magnitude and phase of this signal. Also, what is the phase angle difference between the *I* and *Q* components of this signal?

**Solution:**

The *I* and *Q* signals can be described as

$$I(t) = \sin\left(2\pi 10^9 \cdot t - \pi/5\right)$$
$$Q(t) = \cos\left(2\pi 10^9 \cdot t + \pi/8\right)$$

A plot of these two signals superimposed on the same time scale is shown below:

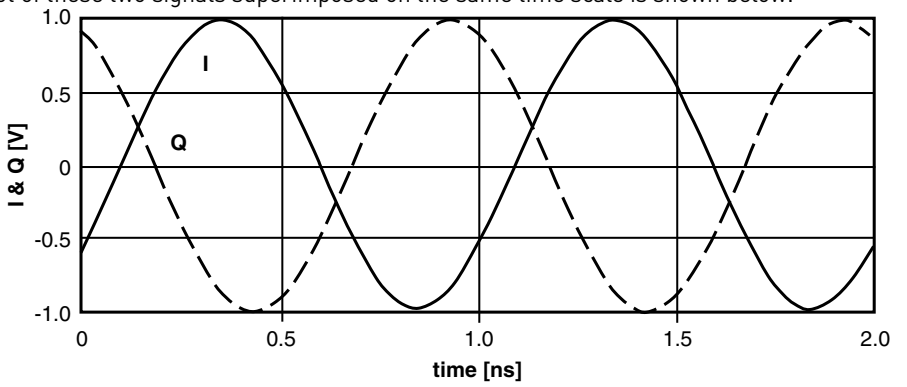


Expressing the complex signal in magnitude and phase form, we write

$$M(t) \cdot e^{j\phi(t)} = \sin\left(2\pi 10^9 \cdot t - \pi/5\right) + j \cdot \cos\left(2\pi 10^9 \cdot t + \pi/8\right)$$

where

$$M(t) = \sqrt{\sin^2\left(2\pi 10^9 \cdot t - \pi/5\right) + \cos^2\left(2\pi 10^9 \cdot t + \pi/8\right)}$$

$$\phi(t) = \tan^{-1}\left[\frac{\cos\left(2\pi 10^9 \cdot t + \pi/8\right)}{\sin\left(2\pi 10^9 \cdot t - \pi/5\right)}\right]$$

A plot of the magnitude and phase of the RF complex signal is shown below:

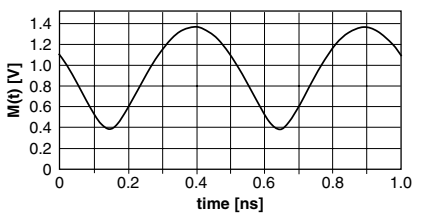


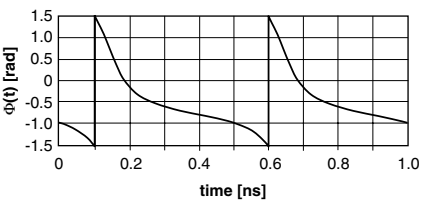


The phase difference between the *I* and *Q* components can be established by rewriting each component in terms of the same trigonometric function, that is, same phase reference point. Since $\cos(x) = \sin(x + \pi/2)$, we can write the *I* and *Q* signals as

$$I(t) = \sin\left(2\pi 10^9 \cdot t - \pi/5\right)$$
$$Q(t) = \cos\left(2\pi 10^9 \cdot t + \pi/8\right) = \sin\left(2\pi 10^9 \cdot t + 5\pi/8\right)$$

Hence, we conclude that the quadrature signal leads the in-phase signal by $33\pi/40$ radians rather than ideal amount of $\pi/2$.

**Figure 13.28.** IQ demodulation.

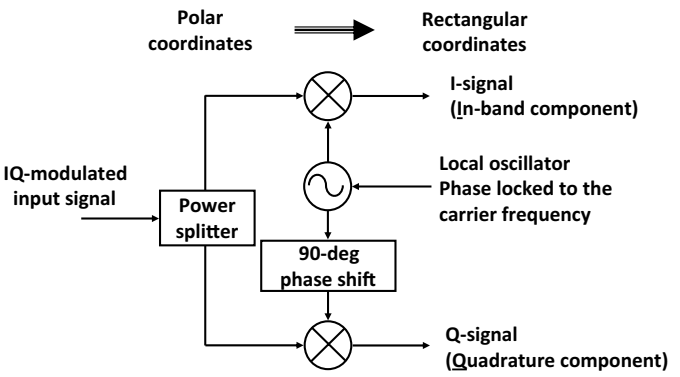


For the receive (RX) path, the phase between the RX_I-BB and RX_Q-BB can be measured. For the TX path, the DUT will be supplied with a perfect *I* and *Q* signal by the ATE, and the embedded IQ signal can be measured after demodulating the RF signal with the ATE.

To measure the phase difference of an RX *I* and *Q* signal, the DUT will be supplied with a CW sinusoidal signal to the RX input, and the output signal will be captured in the time domain. An FFT will calculate the power and the phase of the appropriate signals. The accuracy of the measured phase difference between the *I* and *Q* signal is dominated by the calibration accuracy of the ATE between both measurement channels.

To measure the *IQ* signals in TX mode, it will be necessary to supply the DUT with low frequency *I* and *Q* base-band signals and to analyze the RF signal by digital demodulation. Figure 13.28 shows the block diagram, which needs to be implemented into the test program, either as a firmware routine controlling a DSP engine or directly as a test routine in the program code. The RF signal needs to be captured in the time domain and multiplied with a sine signal with the carrier frequency $\omega_0$ to generate the *I* signal, as well as with a cosine signal to generate the *Q* signal. An FFT can be applied to these signals to capture their corresponding magnitude and phase information.

### 13.5.3 Error Vector Magnitude Test Method

The most widely used figure of merit for modulation quality of digital communication systems is the *error vector magnitude* (EVM) metric. The EVM measurement is sensitive to any signal impairment that affects the magnitude and/or the phase trajectory of the signal. As the name already indicates, EVM is a vector analysis of the error at any given time between an ideal reference signal and a measured signal as shown in Figure 13.29. All the vectors are assumed to be rotating around the origin in a counterclockwise fashion at a rate set by the signal frequency. Here a snapshot of the measured and reference vectors are plotted at a particular point in time. Also shown is the error vector connecting the ends of the measured and reference vectors. It has a magnitude and a phase, Φ. It is the magnitude of this error vector that is related to the EVM metric mentioned above. Also indicated on the drawing is the magnitude and phase difference between the *IQ* measured vector and the *IQ* reference vector. Both the magnitude and angle are different from that which is associated with the error vector. It is important that one does not confuse the "magnitude of the error vector" with the "magnitude error" or the "phase of the error vector" with the phase error, because these two phrases sound so similar.[3,4,5]

**Figure 13.29.** Error vector magnitude (EVM) with reference and measured vector signal at particular point in time, as the vectors are constantly rotating around in a counterclockwise motion at a rate determined by the signal frequency.

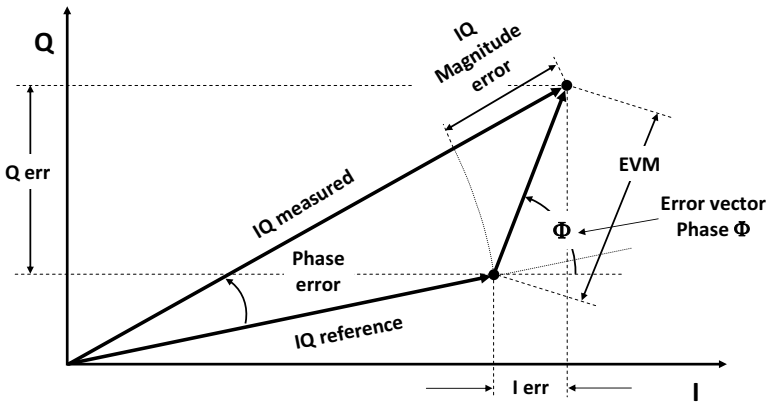


A complex-valued error vector for a particular constellation point can be defined in terms of the corresponding sampled sequence of $I$ and $Q$ components of the measured signal and reference signal as follows:

$$E[n] = \left[I_{measured}[n] - I_{REF}[n]\right] + j\left[Q_{measured}[n] - Q_{REF}[n]\right] \tag{13.101}$$

The EVM metric is defined as the root mean square of the error vector over $N$ samples normalized by a reference power level ($P_{REF}$) as follows:

$$\text{EVM} = \frac{\sqrt{\frac{1}{N}\sum_{n=0}^{N-1}\left|E[n]\right|^2}}{\sqrt{P_{REF}}} \tag{13.102}$$

The reference power $P_{REF}$ level is either the amplitude of the outermost symbol or the square root of the average symbol power. Substituting Eq. (13.101) into Eq. (13.102), we can write EVM as

$$\text{EVM} = \frac{\sqrt{\frac{1}{N}\sum_{n=0}^{N-1}\left\{\left(I_{measured}[n] - I_{REF}[n]\right)^2 + \left(Q_{measured}[n] - Q_{REF}[n]\right)^2\right\}}}{\sqrt{P_{REF}}} \tag{13.103}$$

There are two parts associated with an EVM measurement, the source, and the measurement path. This is depicted in the diagram shown in Figure 13.30. In the source path, the serial data are transformed into a parallel data stream for a multicarrier system. The data are mapped onto the appropriate $IQ$ constellation points and then transformed into the frequency domain. This waveform can be used to modulate an RF source to drive the DUT. The time-domain capture of the DUT output signal is then transformed into a frequency domain signal from which the data are analyzed for its accuracy in regenerating the constellation set.

## EXAMPLE 13.15

The following two *IQ* signals were described in Examples 13.13 and 13.14:

$$x_{measured}(t) = \sin\left(2\pi 10^9 \cdot t - \pi/5\right) + j \cdot \cos\left(2\pi 10^9 \cdot t + \pi/8\right)$$
$$x_{REF}(t) = \sin\left(2\pi 10^9 \cdot t\right) + j \cdot \cos\left(2\pi 10^9 \cdot t\right)$$

Plot the magnitude and phase of vector error sequence between the above two signals.

**Solution:**
As the *I* and *Q* signals of the measured and reference signal can be described as

$$I_{REF}(t) = \sin\left(2\pi 10^9 \cdot t\right), \quad I_{measured}(t) = \sin\left(2\pi 10^9 \cdot t - \pi/5\right)$$
$$Q_{REF}(t) = \cos\left(2\pi 10^9 \cdot t\right), \quad Q_{measured}(t) = \cos\left(2\pi 10^9 \cdot t + \pi/8\right)$$

We compute the vector error *E*(*t*) as

$$E(t) = \left[I_{measured}(t) - I_{REF}(t)\right] + j\left[Q_{measured}(t) - Q_{REF}(t)\right]$$

which, on substituting the given information from above, we write

( ) ( / ) ( ) /

$$M\ t\ = \sqrt{\left[\sin\left(2\pi 10^9 \cdot t - \pi/5\right) - \sin\left(2\pi 10^9 \cdot t\right)\right]^2 + \left[\cos\left(2\pi 10^9 \cdot t + \pi/8\right) - \cos\left(2\pi 10^9 \cdot t\right)\right]^2}$$

$$\phi(t) = \tan^{-1}\left[\frac{\cos\left(2\pi 10^9 \cdot t + \pi/8\right) - \cos\left(2\pi 10^9 \cdot t\right)}{\sin\left(2\pi 10^9 \cdot t - \pi/5\right) - \sin\left(2\pi 10^9 \cdot t\right)}\right]$$

A plot of the magnitude and phase of the error vector is shown below:

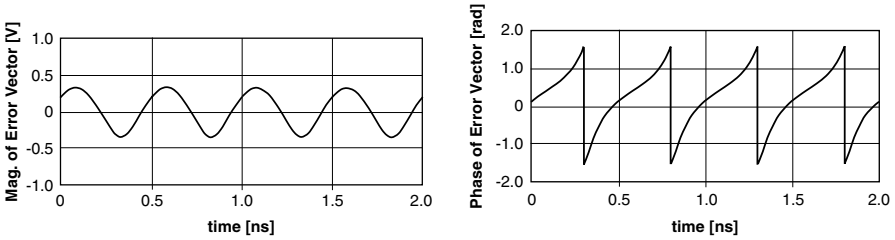


## 13.5.4 Adjacent Channel Power Tests

One other important measurement related to an RF DUT used in a digital communication system is the adjacent channel power (ACP) or the adjacent channel power ratio (ACPR). ACP and ACPR are measures of the leakage power in the adjacent channels normalized with respect to the power in the channel. While an EVM test describes the DUT performance in-band, ACPR is a test that specifies the out-of-band behavior of the DUT. Leakage power influences the system capacity

**Figure 13.30.** Source and measurement path to test EVM.

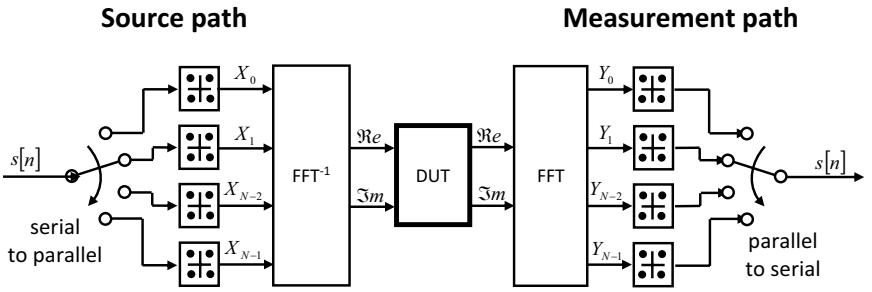


because it interferes with the transmission in the adjacent channels. Therefore, the adjacent channel power or the adjacent channel power ratio test is one of the most common test parameters for production test of an RF transmitter. The ACPR is a measure of the ratio of the wanted channel power to the power in the adjacent and alternate channel due to spectral re-growth. Even though the measurement path is a scalar power measurement, the ATE needs to source the DUT with an *IQ* signal.

Measuring the spectral re-growth of a wideband signal like a WLAN or CDMA signal is one of the most demanding measurements for an ATE. The spectral re-growth is the effect that generates signal power into the adjacent and alternate channel of a particular RF system with defined channels and channel bandwidth. In terms of signal statistics, having a signal leak into an adjacent channel is different than noise in this channel.

In Section 13.1.4, intermodulation distortion was introduced as a measure of the nonlinear performance of a DUT. This measure is still useful here, but the ACPR is a more valuable metric especially for RF systems using a digital modulation scheme. The third-order product of two sinusoidal signals could land in a neighboring channel and cause interference with another signal. Since the modulation becomes more complex, it becomes less obvious that the sinusoidal intermodulation analysis will be adequate for describing the system limitations for complex modulations. Measuring the ACPR with the nominal modulated signal will be the logical extension of the intermodulation distortion measurement. As described previously, IMD is defined as the ratio of the power in one of the third-order tones to that in one of the main tones. ACPR is defined as the ratio of the power in the bandwidth of the channel adjacent to the main signal to the power in the bandwidth within the main signal channel. Alternate channel power ratio (ACP) is also defined in a similar way. It refers to the ratio of the power in a bandwidth two channels away from the main signal to the power in the main channel with the same bandwidth as shown in Figure 13.31. In terms of IMD measurement, a higher-order product like the fifth-order product may be equivalent to the alternate channel power ratio.

While the ACPR measurement is simple to perform in principle, the difficulty of this measurement is due to the complexity of sourcing a defined RF signal into a DUT and measuring the output of the DUT with a high dynamic range without introducing new signal products by the ATE.

### *Modulated Sources*

A key component of the ACPR measurement is the signal source, which needs to provide a standard conformance signal to the DUT. Most of the commercial ATE have a modulated RF source built in, and most of the ATE vendors provide a set of modulated signals for the most common wireless standards. Like IMD or any other distortion measurement, the level of distortion is a very strong

**Figure 13.31.** Adjacent and alternate channel power.

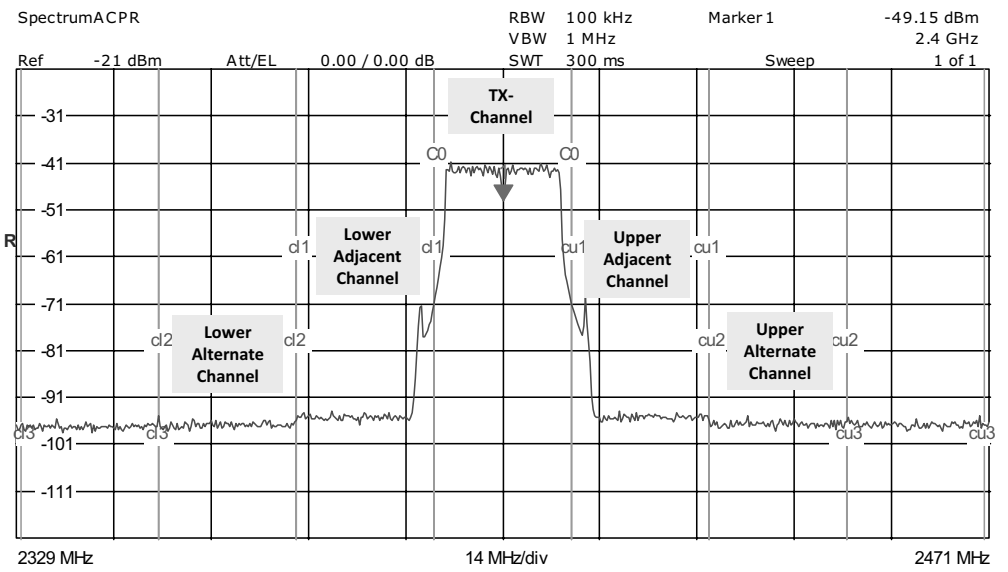


function of the source power level, which might already cause some distortion by the ATE internal source switch matrix and amplification stages. In addition to the power level, ACPR also varies strongly with the modulation format being employed due to the different crest factor associated with the different modulation schemes. It is good practice to verify the ACPR of the ATE sourced signals with bench equipment like a spectrum or signal analyzer with a known performance.

### *Modulation Measurements*

The ATE measurement path architecture needs to be capable of measuring the integrated power in the transmit channel and the adjacent and alternate channels. This will not only require a receiver bandwidth which covers at least the channel bandwidth, but will also need to have a significant dynamic range, which covers the sum of the ACPR power, and crest factor of the modulated signal. In addition, it will be important that the tester's LO will not introduce phase-noise-related signal components.

The dynamic range of the ATE measurement path is at a premium, and the limits must be understood in order to select the optimum ATE settings. The primary constraints are (a) receiver nonlinearities at the high-power end and (b) the measurement path noise floor at the low power end. In addition, the LO phase noise provides a lower bound, but in many cases the measurement path noise floor itself is usually the lower limit. A comparison of the different components that contribute to a ACPR measurement is shown in Figure 13.32.

To measure ACPR, it will be important to follow the specified channel bandwidth and the frequency spacing between the main transmit channel and the adjacent or alternate channel and the filter. Since the ACPR value will vary with the power in the main transmit channel, the channel power will be given as a requirement in the DUT or test specification.

In conclusion, the ACPR measurement is one of the most challenging tests performed on an ATE. The source needs to be modulated with a waveform defined by the specific standard. The dynamic range of the source and measurement path of the ATE will require special attention when correlating the ATE result to bench measured results.

**Figure 13.32.** Parameter impacting the dynamic range of the measurement path of an ATE. The power level will vary for different ATE and ATE settings.

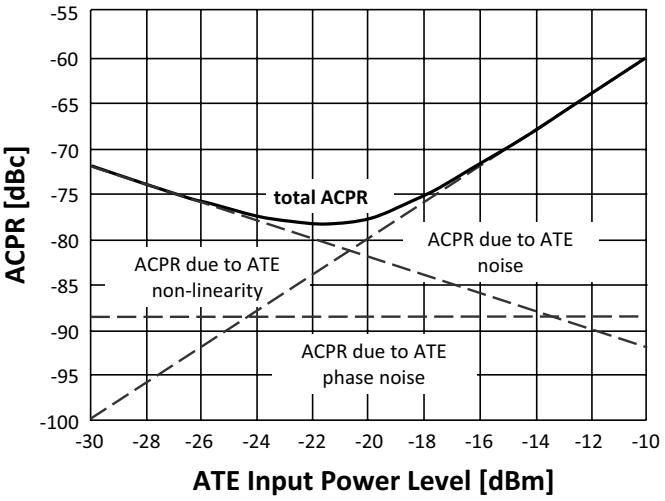


## 13.5.5 Transmit Mask

Spectral mask test is a good indicator of the deteriorating performance of wireless transmission systems for digital modulation schemes like WLAN or cellular phone systems. The DUT is sourced with a standard compliant digitally modulated signal, while the power at the transmit output is measured. The spectral mask test measures the distribution of the transmitted power spectral density similar to the ACPR test. This test makes sure that no unwanted spectral components will be transmitted, which can cause interference in other channels.

When transmitting a digitally modulated signal, all spectral content needs to be below a specified limit or mask. Figure 13.33 shows this mask for a WLAN transmitter.

The reference power level is taken as the peak power spectral density in the signal. The spectral mask applies to frequencies in the frequency band of the adjacent channels. For all offset frequencies, the power spectral density is calculated and compared relatively to the reference level. For all offset frequencies specified in the standard, the power spectral density is tested against a defined mask.

The challenge of this mask test is that the signal bandwidth is already wide for WLAN—for example close to 20 MHz, which is a typical receiver bandwidth of a commercial ATE system. To capture the full mask bandwidth, multiple captures need to be taken, which will increase the test time. The other challenge, which is similar to the ACPR test, is the required dynamic range, which requires a careful selection of the ATE power settings.

## 13.5.6 Bit Error Rate

Bit error rate (BER) is a fundamental system test for measuring a receiver performance, such as the sensitivity and selectivity. The BER is the percentage of erroneous bits received compared to the total number of bits sourced into the receiver during a defined measurement period. While the sensitivity for analog-modulated systems is often specified as the ratio of signal plus noise plus distortion (SINAD), for digital modulated systems and DUT, the sensitivity is specified as the maximum BER for a given sensitivity level. In addition to the power level of the modulated signal, the BER will also depend on in-band and out-of-band interferers and blockers. These interferers

**Figure 13.33.** Transmit spectrum mask for 802.11a.

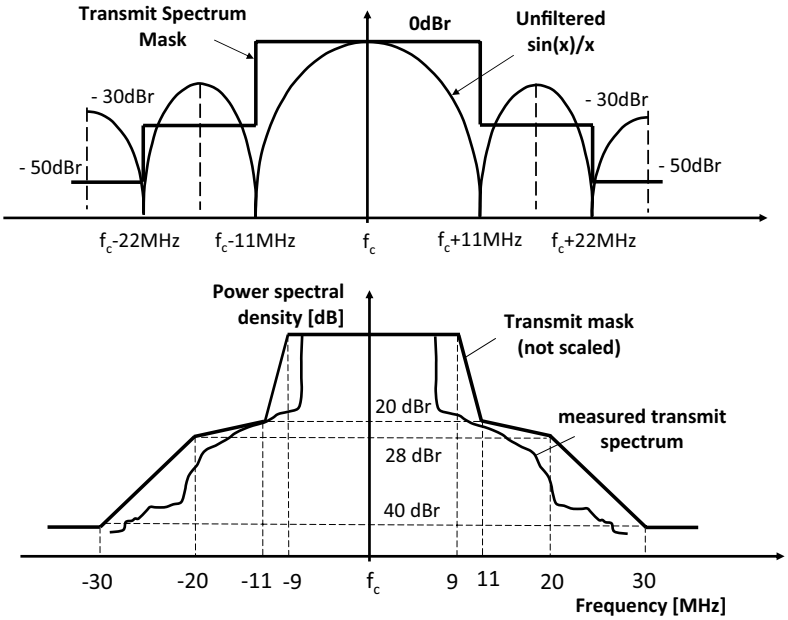


and blockers will simulate data traffic on an adjacent channel, or other strong signals out of band caused by other services. BER is also an efficient metric to specify the quality of the device for these critical parameters.

To perform a BER test, a standard compliant signal is supplied to the input of the receiver, which is modulated with a known pseudorandom bit sequence (PRBS). The analog or digital output will be captured with an analog digitizer, or digital capture using a digital pin.[6] The analog capture can be used to sample an analog as well as a digital bit stream. In the case of the capture of an analog signal, the signal will be digitally demodulated in the ATE DSP, or ATE computer. When capturing a digital bit stream with an analog digitizer, the bits need to be reconstructed and compared with the bit sequence used to modulate the input signal in order to calculate the BER. This method avoids synchronizing the device output with the input in terms of data rate, and thus delaying time caused by the DUT and ATE. Especially for devices without clock recovery circuitry, where the DUT can't trigger the ATE, this method might be the most robust one to implement. With a short known training sequence, the digitized bit stream can be synchronized to the known input signal using a correlation algorithm.

Another method used to measure BER is to capture the digital output of the DUT with the digital capture instrument of the ATE, as shown in Figure 13.34. This method has the advantage of being easily scalable for multisite parallel test setups. Another advantage is that the time delay does not need to be known, since the captured bit stream can be processed using the capture memory, which is synchronized with a matched loop.

The disadvantage of all methods is that the necessary number of bits will require a long bit sequence, which will cause significant test times, especially when data processing is required.

Other methods utilizing on-board test circuits can avoid some of the disadvantages. A built-in XOR circuit can detect failed bits on the flight while the bit sequence is measured by comparing with a known good bit sequence. Another on-board test method would be the implementation of

**Figure 13.34.** BER ATE test set-up.

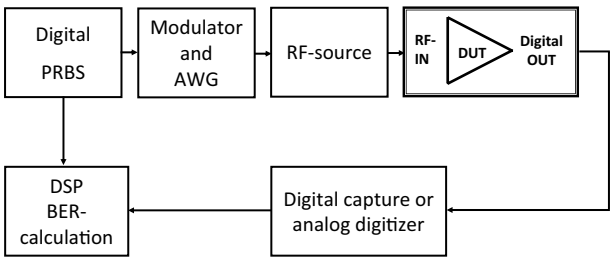


an FPGA. This FPGA could be built as a designated compute engine for the BER test. Additional debug effort will be required when implementing this module for the first time.

Most of the commercial ATEs with RF instrumentations have the capability to combine the signals of at least two RF sources. This enables them to generate the modulated signal on the first RF source with the known bit sequence. The other source can then be used to generate a defined interferer or blocker, and the combined signal can be sourced into the DUT. One typical example for this test is the adjacent channel interference BER test, where a strong modulated signal is transmitted on the adjacent channel. This test condition simulates the real data traffic in a digital RF system.

## 13.6 SUMMARY

In this chapter we reviewed three different types of RF scalar measurements: power, amplitude noise (thermal and 1/*f*) and phase noise, as well as several vector-based tests. We began by describing a typical architecture of the RF portion of an ATE. This was followed by a discussion of the principles of a power measurement using an ATE. Issues relating to dynamic range, maximum power, noise floor, and phase noise were then introduced. A source of error in any RF system is the power loss due to impedance mismatches, transmission losses, and so on, associated with the DIB. To compensate for these errors, de-embedding techniques were introduced. This enables the DUT performance to be separated out from the operation of the DUT-DIB combination. The power measurement techniques can be applied to gain, P1dB, or intermodulation products, as well as the lock-in times of a VCO when its signal dependency with time is taken into account. Several power measurements made with the aid of directional couplers enables one to write a two-port *S*-parameter description of the DUT. The physics of a directional coupler was briefly described where it was shown how to measure the incident and reflected wave at the input and output port of a DUT.

Measurement using an ATE for both the noise associated with a power measurement as well as the phase noise associated with an oscillator output were described. The advantages of the *Y*-factor and cold noise method to measure the noise figure of a DUT were outlined. Phase noise measurements were shown to be made with methods like the PLL- and delay-line phase noise method instead of the commonly used bench-top approach using a spectrum analyzer.

In the last part of this chapter we studied the principles of a vector signal analysis. Since a standard RF ATE has all the building blocks of a vector signal analyzer, it was shown how an ATE could be used to measure more complex RF system parameters like EVM, ACPR, and BER. Common to all these tests is that the stimulus needs to be a modulated signal.

An important lesson derived from this chapter is that the DUT, the DIB, and the ATE must be treated as an RF system rather than a cascade of three independent electrical elements. This requires the test engineer to design the test system in much the same way that the system designer would design a new device or RF system. System parameters like dynamic range, maximum power, signal

bandwidth, measurement bandwidth, noise figure, noise bandwidth, phase noise, compression point and gain distribution in the source and measurement path all need to be considered by the test engineer during the initial DIB design phase. It is the goal of the test engineer to develop an RF test program using an ATE such that the test results match the results of a dedicated RF measurement equipment, like a spectrum analyzer, RF synthesizer, vector signal analyzer, or network analyzer.

## PROBLEMS

**13.1.** What are the major blocks of an spectrum analyzer?

**13.2.** What are the major blocks of an RF ATE measurement path with an zero IF architecture?

**13.3.** Why can the the dynamic range of a spectrum analyzer be large compared to a vector signal analyzer?

**13.4.** What can happen if the maximum expected power of an ATE measurement path is set too low?

**13.5.** What can happen if the maximum expected power of an ATE measurement path is set too high?

**13.6.** What condition is required for coherent sampling and what happens if this condition is not true for a phase noise measurement?

**13.7.** What IF frequency should be selected for a ZIF ATE architecture to be coherent with an ADC having a sampling rate of 50 MHz, if 1024 samples are required for FFT processing and the output of the mixer ranges between 15 and 20 MHz?

**13.8.** A 2.5-GHz RF signal is to be down converted by a mixer and directed to a digitizer for digital conversion. If the digitizer is sampled at a clock rate of 100 MHz and 2048 samples are collected for digital signal processing using an FFT, what should be the local oscillator frequency if the mixer has an output IF frequency range between 15 and 20 MHz?

**13.9.** A gain test was performed on a DUT and found to be 21.3 dB. The DUT is connected to an ATE through an interface board with an operating loss of 2.1 dB. What is the actual gain of the device?

**13.1.** A gain test was performed on a DUT using an ATE with an interface board. The gain was found to be 11.4 dB. If the source, the meter, and the input and output ports of the DUT have return losses of 10, 12, 13, and 12 dB, respectively, and the traces introduce losses totaling 0.45 dB, what is actual gain of the DUT?

**13.2.** What is the operating loss associated with the input-side of an interface board shown in Figure 13.6 if the following measurements at the input port of the board were obtain using the in-socket calibration method, together with a single DUT measurement:

$$S_{11,DUT} = 0.21 - j0.32, \quad S_{11,open} = -0.85 + j0.32$$
$$S_{11,short} = 0.85 - j0.12, \quad S_{11,load} = 0.53 - j0.31$$

**13.3.** For the measurements made in problem 13.11 above, what is the input impedance of the device under test?

**13.4.** What is the operating loss associated with the output side of an interface board shown in Figure 13.6 if the following measurements at the output port of the board were obtain using the in-socket calibration method, together with a single DUT measurement:

$$S_{11,DUT} = 0.21 + j0.22, \quad S_{11,open} = -0.89 + j0.13$$
$$S_{11,short} = 0.9 + j0.13, \quad S_{11,load} = 0.15 - j0.31$$

**13.5.** For the measurements made in Problem 13.13 above, what is the output impedance of the device under test?

**13.6.** A gain test was performed on a device under test and found to be 19.3 dB. The input port to the load board was measured using a vector network analyzer under four separate calibrated conditions, resulting in

$$S_{11,DUT} = 0.11 - j0.22, \qquad S_{11,open} = 0.91 + j0.12$$
$$S_{11,short} = -0.54 + j0.21, \quad S_{11,load} = 0.35 - j0.13$$

What is the true gain of the device if the output signal path has zero losses? What is the input impedance of the DUT?

**13.7.** Why is the IP3 of an RF system so important?

**13.8.** What is the slope of the second- and third-order response in the input/output power diagram? What is the mathematical background for these slopes?

**13.9.** The intermodulation distortion measurements are made at a –10-dBm output-power level per fundamental tone. The intermodulation distortion products power level is at –73 dBm per tone, and the power level for the fundamental tones is –5 dBm. What is the third order intercept point?

**13.10.** The spectrum below has been measured when supplying an amplifier with a 20 dBm per tone two-tone signal. What is the OIP3, the IIP3, and the gain of this amplifier?

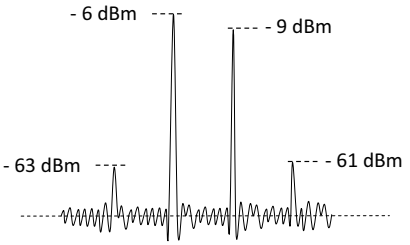


**13.11.** Name four methods used to measure the compression point of an RF system like an amplifier.

**13.12.** What advantages does the modulation method have when measuring the compression point?

**13.13.** The following measurments of amplifier gain expressed in decibels were found using 2 dBm increasing steps of input power beginning at –10 dBm: 11.92, 11.81, 11.35, 10.98, 10.13, 9.89, 9.35, 8.76. The small-signal gain was measured previously and found to be equal to 11.35 dB. What is the 1-dB compression point of this amplifier using interpolation with a a linear rule of gain behavior aaround the P1dB. How does this result compare with an interpolation method that uses a polynomial approximation of the data set?

**13.14.** The gain of an amplifier was found through interpolation to depend on its input power over a 0- to 10-dBm range according to

$$G = 0.1 + 10.2 \times P_{in} + 0.1 \times P_{in}^2$$

What is the 1-dB compression point associated with this amplifier if the nominal small-signal gain is 10 dB?

**13.15.** The minumum P1dB is listed in a device data sheet to be –10 dBm. A gain test is performed for an input of –30 dBm and the gain is found to be 15.3 dB. A second test is

performed at –10 dBm and the gain is found to be 14.25 dB. Does this device pass its 1-dB compression point test?

**13.16.** Name the two most common methods used for measuring the noise figure with an ATE, and what are the advantages and disadvantage of each method. Why can the the dynamic range of a spectrum analyzer be large compared to a vector signal analyzer?

**13.17.** Why is it important to pay special attention to the load condition when using a noise source with a high ENR value?

**13.18.** What is the NF of a DUT if the noise source has an ENR of 21 dB and the hot and cold noise power is –101.2 dBm and –119.1 dBm, respectively?

**13.19.** What is the noise factor of a DUT if the noise source has an ENR of 34 dB and the *Y*-factor is 500?

**13.20.** What is the peak power level expected at the output of a DUT if it has an NF of 5 dB, the noise source has an ENR = 28 dB and the effective bandwidth of the measurement path is 0.75 MHz. The cold noise is assumed to be equal to thermal noise at T = 275 K.

**13.21.** The phase noise of an oscillator at an offset of 100 kHz from the carrier is equal to –96 dBc/Hz. Assuming that the noise process is best described as Lorentzian, write a general description of the phase noise as a function of frequency.

**13.22.** The phase noise of a VCO needs to be tested. A 320-MHz reference signal is sourced from an ATE to a PLL with a feedback divider ratio of 64. If the ATE reference has a phase noise of –125 dBc/Hz, what is the minimum level of VCO phase noise that can be measured with this setup? Assume that the VCO phase noise should be at least 10 dB greater than the reference noise contribution.

**13.23.** The phase noise of a VCO within a PLL with a feedback divider ratio of 64 is to be tested using a delay-line phase noise test setup. The VCO is to be tuned to a frequency within the ISM frequency band at 5.750 GHz, and the phase noise is to be measured at approximately 1-MHz offset. What frequency should be sourced to the PLL from the ATE, and what sampling frequency should the digitizer use to collect 4096 samples? What is the exact offset frequency from the VCO output?

**13.24.** The phase noise of an oscillator is to be tested using a PLL-based phase noise test setup. The oscillator is tuned to a frequency of 1.401367 GHz. What is the phase noise of this device at a frequency offset of 4.8828 MHz if the output is digitized at a sampling rate of 5 GHz using an ADC with an input impedance of 50 Ω. Subsequently, a 1024-point FFT analysis reveals the following information:

$$\text{FFT}\left\{x[n]\right\} = \begin{cases} 3.42\times10^{-4} & \text{Bin} = 0 \\ \vdots & \\ 2.32 & \text{Bin} = 4710 \\ 7.56\times10^{-3} & \text{Bin} = 4711 \\ 6.20\times10^{-3} & \text{Bin} = 4712 \\ \vdots & \end{cases}$$

**13.25.** What are the main blocks of a vector signal analyzer, and why is it similar to an RF ATE?

**13.26.** Why does the error vector magnitude (EVM) describe the transmit function of an RF system in a single figure of merit?

**13.27.** A 5-GHz continuous wave sinusoidal signal is passed through a quadrature modulator resulting in an IQ signal having the following form: $\sin(\pi 10^{10}\cdot t+\pi/12)+j\cdot\cos(\pi 10^{10}\cdot t-\pi/10)$.

What is the magnitude and phase of this signal. Also, what is the phase angle difference between the *I* and *Q* components of this signal?

**13.28.** The following IQ signal was generated by a quadrature modulation process $0.95\sin(2\pi f_o \cdot t - \pi/7) + j \cdot 1.1\cos(2\pi f_o \cdot t + \pi/8)$. If the reference is described by $\sin(2\pi f_o \cdot t) + j\cos(2\pi f_o \cdot t)$, what is the vector error associated with the signal? Plot its magnitude and phase as a function of time for $f_o$ equal to 900 MHz.

## REFERENCES


1. Agilent, *Vector Signal Analysis Basics*, Application Note 150-15, Agilent Technologies, Inc., 2004.
2. M. Hiebel, *Fundamentals of Vector Network Analysis*, Rohde & Schwarz, Beaverton, 2007.
3. G. Srinivasan, H-C. Chao, and F. Taenzler, *Octal-site EVM tests for WLAN transceivers on* very low-cost ATE platforms, in *Proceedings of the IEEE International Test Conference*, 2008.
4. 802.11a-1999. *Supplement to IEEE standard for information technology telecommunications and information exchange between systems-local and metropolitan area networks-specific requirements.*
5. Agilent Technologies Application Note 1380-1, *RF Testing of WLAN Products.*
6. K. B. Schaub and J. Kelly, *Production Testing of Rf and System-on-a-Chip Devices for Wireless Communications*, Artech House, Boston, 2004.